Chemical Science

ROYAL SOCIETY OF CHEMISTRY

EDGE ARTICLE

View Article Online
View Journal | View Issue

Cite this: *Chem. Sci.*, 2025, **16**, 255

All publication charges for this article have been paid for by the Royal Society of Chemistry

Received 11th August 2024
Accepted 8th November 2024

DOI: 10.1039/d4sc05396f

rsc.li/chemical-science

Pronounced electronic modulation of geometrically-regulated metalloenediyne cyclization†

Sarah E. Lindahl,[a] Erin M. Metzger,[a] Chun-Hsing Chen,[b] Maren Pink[b] and Jeffrey M. Zaleski *[a]

Using a diverse array of thermally robust phosphine enediyne ligands (dxpeb, X = Ph, Ph-*p*OCH_3, Ph-*p*CF_3, Ph-*m*$_2CH_3$, Ph-*m*$_2CF_3$, ^{i}Pr, Cy, and ^{t}Bu) a novel suite of cisplatin-like Pt(II) metalloenediynes (**3**, Pt(dxpeb)Cl_2) has been synthesized and represents unique electronic perturbations on thermal Bergman cyclization kinetics. Complexes **3e** (Ph-*m*$_2CF_3$) and **3f** (^{i}Pr) are the first of this structure type to be crystallographically characterized with inter alkyne termini distances (**3e**: 3.13 Å; **3f**: 3.10 Å) at the lower end of the widely accepted critical distance range within which enediynes should demonstrate spontaneous ambient temperature cyclization. Despite different electronic profiles, these metalloenediynes adopt a rigid, uniform structure suggesting complexes of the form Pt(dxpeb)Cl_2 have orthogonalized geometric and electronic contributions to thermal Bergman cyclization. Kinetic activation parameters determined using ^{31}P NMR spectroscopy highlight the dramatic reactivity and thermal tunability of these complexes. At room temperature, the half-life ($t_{1/2}$) of cyclization spans a range of ~35 hours and for the aryl phosphine derivatives, cycloaromatization rates are 10–30 times faster for complexes with electron donating substituents (**3b**: Ph-*p*OCH_3; **3d**: Ph-*m*$_2CH_3$) compared to those with electron withdrawing substituents (**3c**: Ph-*p*CF_3; **3e**: Ph-*m*$_2CF_3$). Computational interrogation of the aryl phosphine metalloenediynes **3a–3e** reveals that the origin of this precise electronic control derives from electronic withdrawing group-mediated alkyne carbon polarization that amplifies coulombic repulsion increasing the cyclization barrier height. Additionally, mixing between the in-plane π-orbitals and the phosphine aryl ring system is pronounced for complexes with electron donating substituents which stabilizes the developing C–C bond and lowers the activation barrier. This π-orbital mixing is negligible however, for complexes with electron withdrawing substituents due to an energetic mismatch of the orbital systems. Overall, this work demonstrates that for geometrically rigid frameworks, even remote enediyne functionalization can have pronounced effects on activation barrier.

Introduction

Over 30 years ago, the discovery of the unprecedented, enediyne-containing natural products[1–6] introduced the world to the biologically active 1,5-diyne-3-ene functionality whose seemingly esoteric cyclization reactivity was described by Masamune[7] and Bergman[8] over a decade prior. Currently, 14 enediynes and 5 cycloaromatized compounds have been structurally characterized,[9–17] verifying the unique diyne-ene motif that generates the reactive 1,4-phenyl diradical species responsible for biological potency. Despite being known for decades, enediynes are still on an upward trajectory and have not yet reached their peak impact. As evidence, two second-generation antibody-conjugated forms of calicheamicin (Mylotarg and Besponsa) have been approved by the FDA (Mylotarg reapproved) in 2017 and show low nanomolar-to-picomolar activity against acute myeloid and lymphoblastic leukemias.[10,18,19] Other enediyne-containing conjugates have been approved outside the US or are currently in development and show cytotoxicity limits in comparable ranges.[20–22] The success of these natural product conjugates is a triumph for a class of molecules that has struggled to maintain a presence in mainstream medicinal chemistry. Yet, there are still extensive unmet challenges: many natural product enediynes react too quickly at ambient temperature to be directly drugable,[10] suites of synthetic analogues with delicately tuned reactivity do not yet exist, and the role of the enediyne unit in nature is not even well-

[a]*Department of Chemistry, Indiana University, Bloomington, IN 47405, USA. E-mail: zaleski@iu.edu*

[b]*Molecular Structure Center, Indiana University, Bloomington, IN 47405, USA*

† Electronic supplementary information (ESI) available: The data supporting this article including crystallographic data, DSC traces, kinetic measurements, and Cartesian coordinates and vibrational frequencies of computed structures. CCDC 2083580–2083585 and 2083637–2083642. For ESI and crystallographic data in CIF or other electronic format see DOI: https://doi.org/10.1039/d4sc05396f

defined. Many of these shortcomings survive because researchers have yet to fully understand and harness the geometric and electronic structural parameters responsible for the fundamental reactivity of the 1,5-diyne-3-ene unit to effectively put constructs beyond natural product enediyne-conjugates to appropriate use.

One of the most fundamental paradigms describing the base reactivity of enediynes was established by Nicolaou *et al.* early on in the field's development and stated that a critical distance (*d*) between alkyne termini existed at which spontaneous enediyne cyclization would occur (*d*: 3.2–3.31 Å).[23,24] Computational analysis by Schreiner later supplemented these findings and expanded the critical distance range, especially the lower limit, to 2.9–3.4 Å.[25] Work by Snyder,[26,27] and later in conjunction with Magnus,[28] also added that differential strain between the ground and transition states contributes significantly to the kinetics of cycloaromatization for more complex ring-closed systems.

Electronic perturbations of the enediyne framework have also been shown to influence Bergman cyclization kinetics. Modulation of orbital contributions and energetic dependencies are inherently system-specific and can lead to complex trends in reactivity outcomes. For example, Semmelhack *et al.* demonstrated that incorporation of the –ene– unit into an aromatic ring stabilizes the base enediyne framework significantly and reduces cyclization reactivity.[29,30] In a similar vein, Jones and others have shown that functionalization of the vinylic positions with σ-donating or σ/π-withdrawing groups leads to enhancement or retardation of cyclization, respectively,[31,32] due to differential electron repulsion in the developing diradical transition state. This result is at first glance counterintuitive since electron withdrawing substituents, inductively or through space, should decrease the observed electrostatic interaction. It can only be rationalized by the structural disposition of the lone pairs and their field effect[32] relative to the developing diradical and C2···C7 bond. An analogous polarization argument was employed by Schmittel *et al.* to explain differential barrier heights as a function of alkyne termini substituent. Here, however, distal *p*-phenyl substituted electron withdrawing groups play a more traditional inductive role in reducing the electron repulsion in the transition state thus lowering the activation barrier to Bergman cyclization.[33] This result was later supported and enhanced by Schreiner *et al.* who showed that σ-withdrawing functionalities (or π-donors) directly at the alkyne termini engender a parallel stabilizing influence on the transition state structure by facilitating the formation of the benzenoid diradical intermediate leading to rate acceleration.[34] It is clear from these demonstrations that electronic effects are complex and influenced by both pure electronic (*i.e.*, inductive) as well as spatial (*i.e.*, proximity) interactions between populated orbitals. These effects, while significant, are superimposed upon a given geometric structural reactivity base and further modulate the observed Bergman cyclization rate.

To further harness the geometric component of the activation, metal fragment complexation was first realized in the mid-1990s to provide a highly dynamic, conformational platform for activating bound enediyne substrates. Buchwald and coworkers developed the acyclic enediyne 1,2-bis((diphenylphosphino) ethynyl)benzene (dppeb) as a ligand for d^8 Pd(II) and Pt(II) which generates a square planar geometry and is computationally determined to have a significantly reduced inter alkyne termini separation of 3.3 Å.[35] This translates to spontaneous thermal reactivity in solution at ambient temperature for these complexes *in situ*, consistent with the original cyclization paradigm put forth by Nicolaou.

While an ensemble of geometrically-modulated, metal-mediated Bergman cyclization demonstrations exist, there are far fewer examples of electronic influences on metal-modulated enediyne frameworks.[36,37] The thermal cyclization of a Mo(IV) dithiolate–enediyne complex is one of them. Here the high-valent metal fragment stabilizes the sulfur lone pairs which eliminates electron repulsion with the developing diradical species in the transition state. This stabilization lowers the activation barrier to cyclization as had been previously demonstrated for the purely organic examples by an analogous mechanism.[37] Although this example relies directly on the electronics of the metal fragment to influence the cyclization rate, what we have learned from the organic enediyne reactivity demonstrations is that substitution of the ligand framework can also have significant electronic contributions that modulate the geometry-controlled reactivity set point.

More than a quarter century has passed since Nicolaou,[23,24] Schreiner,[25] Buchwald,[35] and others demonstrated that there exists a crude geometric critical distance for seemingly disparate enediyne structures to react spontaneously, and this paradigm has held ever since. Similarly, it has been nearly as long since electronic influences on enediyne cyclization have been established on somewhat independent frameworks.[26–34] Herein we show that for a Pt(dxpeb)Cl_2 derivatized suite, these two control mechanisms can be selectively merged to enhance the rate of thermally stable constructs or stabilize otherwise spontaneously reactive molecules. A key outcome of this systematic approach is that molecular structures that fall at the lower end of the historical critical distance threshold now can be crystallized and their structures elucidated in detail, while those that should be reactive according to that same tenet are stabilized for extended periods due to the electronic counterbalance.

Results and discussion

Functionalized phosphine enediynes and oxide derivatives

We set to synthesizing a diverse array of phosphine enediyne ligands bearing both aryl (**a**: Ph, **b**: Ph-*p*OCH_3, **c**: Ph-*p*CF_3, **d**: Ph-*m*$_2CH_3$, and **e**: Ph-*m*$_2CF_3$) and alkyl (**f**: ^{i}Pr, **g**: Cy, and **h**: ^{t}Bu) substituents to better understand the ways in which electronic substitutions at the alkyne termini work to modulate the activation barrier to thermal Bergman cyclization. The ligands **1b–1h** were synthesized from a modified procedure established for the phenyl-substituted phosphine enediyne **1a**.[35] Generally, to a solution of the TMS-protected precursor enediyne is added *n*-BuLi and the reaction mixture heated to achieve deprotection of the alkyne. Subsequently, addition of the appropriate $ClPR_2$ reagent leads to isolation of the crude R-group-substituted

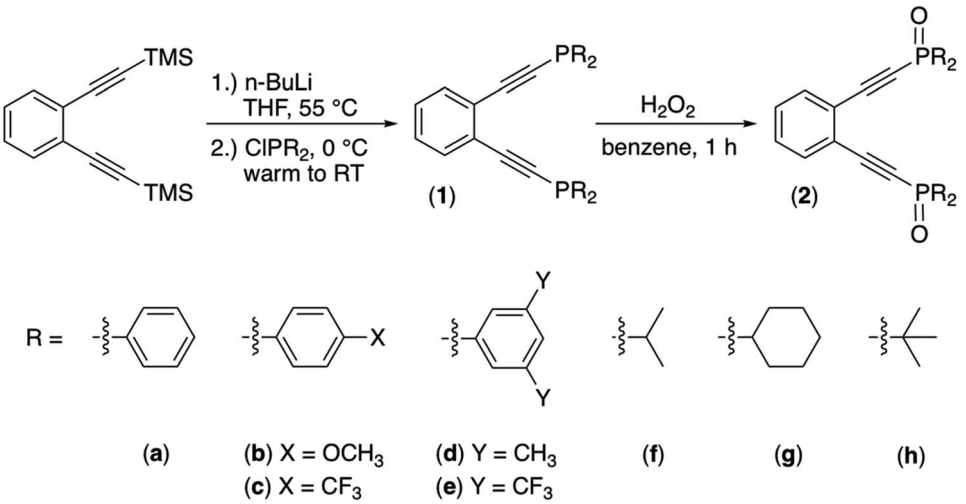

Scheme 1 Synthesis of phosphine enediynes (**1a–1h**) and phosphine oxide derivatives (**2a–2h**).

phosphine enediyne (Scheme 1). Purification with silica gel flash chromatography affords these ligands as either pale yellow solids (**1a–1b** and **1d–1e**) or as yellow oils (**1c** and **1f–1h**). The phosphine oxide analogues (**2a–2h**) were intentionally synthesized by the addition of hydrogen peroxide to a solution of enediyne **1a–1h** and their spectroscopic signatures identified, providing a valuable tool to monitor the oxidation of the enediyne ligands **1a–1h**.

Evaluating the ^{31}P NMR chemical shifts of the enediyne ligands allows us to visualize the extent to which functionalization of the alkyne termini perturbs the chemical environment of the phosphine. Phosphorus chemical shifts are influenced by the distribution of electron density in the σ-bonds between the phosphorus atom and its substituents, the degree of π-bonding, and variations in the C–P–C angles, which provide information about phosphine basicity.[38] Clearly, derivatization with aromatic (**1a–1e**) and aliphatic (**1f–1h**) functional groups yields a wide range of ^{31}P NMR resonances ($\Delta\delta$ ~50 ppm). Despite this breadth, all enediynes bearing aryl substituents show ^{31}P NMR shifts < 5 ppm of one another suggesting that the presence of electron donating and withdrawing groups at various positions on the terminal phenyl rings does not modulate the basicity of the phosphine to a considerable extent.

Reducing the flexibility of the phosphine by forming phosphine oxide analogues **2a–2h** suppresses the variations in the C–P–C angles, minimizing steric influences on chemical shift, and allowing for isolation of electronic influences.[38] As with enediynes **1a–1h**, large chemical shift differences (>35 ppm) are observed between the aromatic (**2a–2e**) and aliphatic substituents (**2f–2h**), with the most electron donating R-groups appearing downfield. For the suite of aryl-substituted ligands, differences in ^{31}P NMR chemical shift are small (<7 ppm); however, a clear trend is observed as a function of electron donating ability which is a mixture of both inductive (σ) and resonance (π) effects: **2e** < **2c** < **2a** < **2b** < **2d**. Functionalization of the aromatic rings at the alkyne termini with electron donating groups minimally increases the basicity of the phosphine while the presence of electron withdrawing groups decreases basicity. While these effects are not as pronounced as those observed between aromatic and aliphatic R-groups, they do demonstrate that aryl ring substitution can be used to subtly tune the electronic nature of the phosphine.

The phosphine oxide ligands **2a–2h** are stable when stored under ambient conditions while the enediyne ligands **1a–1h** show no degradation over >9 months when stored as solids or dilute solutions in air at 0 °C. The robustness of these phosphine enediynes is reflected in their Bergman cyclization temperatures as measured by differential scanning calorimetry (DSC). For enediyne frameworks, endothermic events are consistent with melting while exothermic events are indicative of cycloaromatization.[35,39–42] Though these studies were performed with neat material in the absence of a radical quenching agent, they provide a relative measure of the activation barrier to cycloaromatization, and when coupled with other structural information, can be used to predict the reactivity of enediyne-containing constructs towards Bergman cyclization in solution.

DSC traces have been obtained for aryl substituted enediynes **1a–1b** and **1d–1e** which melt between 78–144 °C and then cyclize in the liquid phase between 264–275 °C (Fig. 1S†). Though the range of melting is large (>60 °C), the cyclization window is quite narrow (11 °C). In this case, the presence of electron donating or withdrawing groups on the aromatic rings does not lead to a substantial change in the thermal activation barrier to Bergman cyclization. However, ligands whose phosphine termini have been functionalized at both *meta* positions (**1d–1e**) show higher melting temperatures than those bearing no functionalization (**1a**) or substitution only in the *para* position (**1b**), suggesting that differences in solid-state packing may inhibit melting of these phosphine enediynes. The cyclization temperatures of the phosphine oxide analogues are markedly higher than those of the non-oxidized ligands. In general, the melting temperature increases between 20–80 °C upon oxidation and no cyclization events are observed below 280 °C for ligands **2a–2b** and **2d–2e**.

Alkyne termini separations from X-ray crystallography can be used to predict relative activation barriers to diradical generation in simple enediyne systems. Ligands **1d–1e** and **2d–2e** were obtained as crystalline products from vapor diffusion of hydrocarbon solvents into saturated dichloromethane solutions at −20 °C and analyzed using X-ray crystallography (Fig. 1). Though **1a** has been modeled computationally,[35] **1d–1e** and **2d–2e** represent the first phosphine enediyne ligands to be crystallographically characterized.

Enediynes **1d** and **1e** feature aryl rings at the phosphine termini which have been substituted in the *meta* positions with $-CH_3$ and $-CF_3$ groups, respectively. Both ligands show a high degree of π-stacking between the aromatic rings bound to the phosphorus atoms, with the closest points of contact between these stacked rings being ∼3.7 Å (**1d**) and 3.9 Å (**1e**). The presence of these non-covalent interactions supports the proposal that differences in solid-state interactions lead to variance in the DSC melting temperatures of these enediyne ligands. The two arms of the enediyne moiety are symmetric in **1e** showing identical C–C≡C and C≡C–P angles while those of **1d** show a high degree of asymmetry (Table 1S†). For both ligands, the alkyne termini separations are large (**1d**: 4.09 Å; **1e**: 4.20 Å) and compare favorably with the computed distance of **1a** which has been reported as 4.1 Å.[35] The structures of the phosphine oxide analogues **2d** and **2e** have also been crystallographically determined and, though similar to their non-oxidized counterparts, show some unique differences from **1d** and **1e**. The inter alkyne termini distance of **2d** is greater than that of **1d** by ∼0.12 Å.

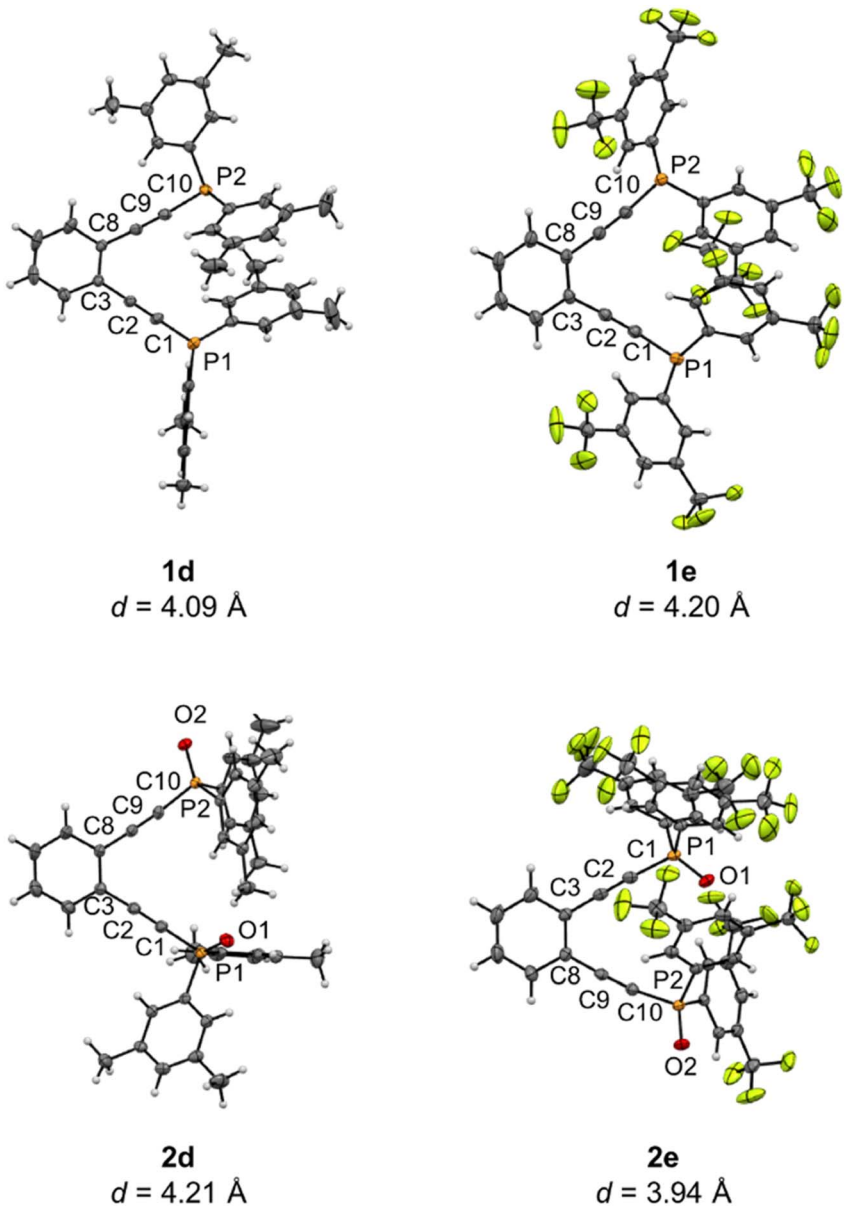

Fig. 1 X-ray crystallographic structures of phosphine enediynes (**1d** and **1e**) and phosphine oxide analogues (**2d** and **2e**). Thermal ellipsoids are illustrated at 50% probability and interalkynyl distances (*d*) are given below structures.

Oxidation at the phosphine leads to changes in structure at the alkyne termini resulting in a widening of the enediyne framework. Interestingly, the interalkynyl distance of **2e** is reduced by ~0.26 Å relative to **1e**. Here, one of the alkyne arms has rotated the bulky $-CF_3$ substituted rings to the exterior of the enediyne framework lessening the steric clash between the large aromatic substituents. Overall, these structural data are consistent with the high cyclization temperatures observed in the DSC analyses and highlight the geometric similarities between these substituted phosphinoenediynes.

Isolation of sensitive Pt(II) phosphine enediyne dichloride complexes

Using this suite of functionalized phosphine enediynes, we synthesized a series of square planar platinum(II) complexes, **3a–3h**, bearing these ligands. Buchwald's original report for the *in situ* formation of **3a** showed spontaneous solution cyclization at room temperature.[35,43] Within this well-defined geometric framework, we recognized the opportunity to investigate how unexplored electronic modifications at the phosphine termini can lead to acceleration or retardation of ambient temperature Bergman cyclization kinetics.

Compounds **3a–3g** have been successfully synthesized and spectroscopically characterized, representing the first Pt(II) phosphine enediyne suite isolated to date. For all compounds except **3d**, addition of 1.2 equivalents of phosphine enediyne to a solution of dichloro(1,5-cyclooctadiene)platinum(II), Pt(cod)Cl_2, in dichloromethane affords the desired metalloenediynes as pale-yellow solids (Scheme 2). In the synthesis of **3d**, a slight excess of metal precursor is required to isolate the intended Pt(II) phosphine enediyne product. Successful synthesis of **3a–3g** required optimization of reaction times and temperatures in all cases. These synthetic changes suggest that R-group modifications of the phosphine ligands may have substantial consequences on metalloenediyne reactivity as some complexes such as **3b** were unstable if isolated at room temperature while others such as **3f** required prolonged reaction times at 25 °C. Though complex **3h** bearing the *tert*-butyl-substituted phosphine enediyne was observed *in situ* by NMR spectroscopy, attempts to isolate this complex proved unsuccessful.

The crude solids of **3a–3g** isolated directly from the reaction mixtures contained Pt(cod)Cl_2 impurities by ^{1}H NMR spectroscopy. Alteration of the synthetic conditions to eliminate this impurity was ineffective for all complexes, and in many instances resulted in the formation of intractable material if reaction times and/or temperatures were increased. Consequently, these metalloenediynes were purified to give pale-yellow solids either through preparatory silica chromatography (**3a–3b**, **3d**, and **3f–3g**) or repeated washings with diethyl ether (**3c** and **3e**). Attempts to purify the fluorinated metalloenediynes **3c** and **3e** using chromatography led to the degradation of these complexes on the chromatographic substrate. This was unanticipated as the fluorinated ligands **1c** and **1e** are repeatedly purified by this method with no evidence of enediyne degradation. Once purified, compounds **3c** and **3e–3g** are stable for ~10 days at −20 °C. In contrast, metalloenediynes **3a–3b** and **3d** degrade significantly upon standing at −20 °C for ~48 h.

Interestingly, addition of a slight excess of **1d** to a solution of Pt(cod)Cl_2 in dichloromethane affords not the monomeric complex **3d** (^{31}P δ = −16.53 ppm), but rather the dimeric complex **5d** (^{31}P δ = −2.61 ppm) (Scheme 3). X-ray crystallography reveals **5d** to have two equivalents of $PtCl_2$ bridged by two molecules of the phosphine enediyne **1d** generating a C_2-symmetric dimer. The inter alkyne termini distance of **5d** which has the methylated ligand **1d** bridging two platinum centers is exceptionally large at 4.53 Å which suggests that this dinuclear complex is thermally robust (Table 2S†). There is significant distortion from linearity in the C–C≡C and C≡C–P bond angles which measure 168 and 163°, respectively, to accommodate bridging both platinum centers. The differential scanning calorimetry trace of **5d** shows no exothermic event indicative of cyclization up to 280 °C which is consistent with the large alkyne termini separation. Incubation of **5d** with excess 1,4-cyclohexadiene (1,4-CHD) at room temperature shows no reactivity over the course of 72 h when monitored by NMR spectroscopy, confirming that this dinuclear complex has a high activation barrier to diradical generation due to the

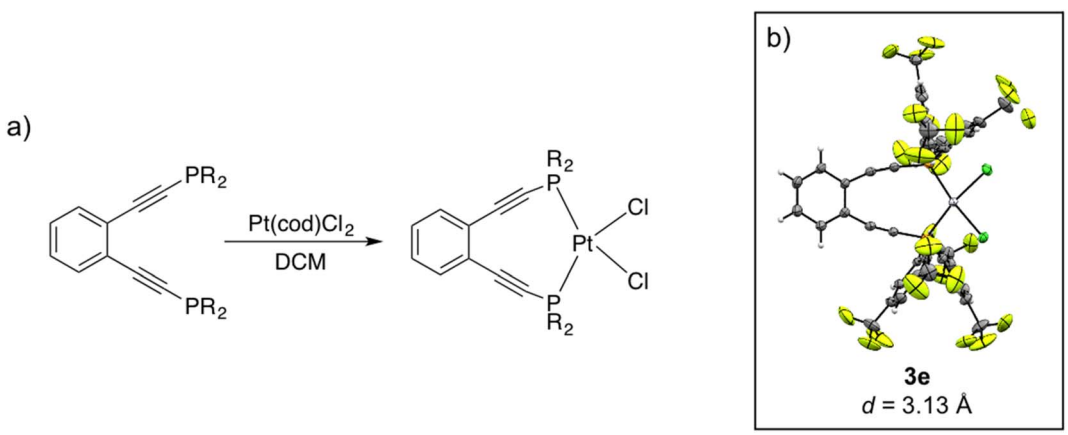

Scheme 2 (a) General synthesis of Pt(II) phosphine enediyne dichloride complexes (**3a–3g**). (b) X-ray crystallographic structure of **3e** with interalkynyl distance (*d*) shown below. Thermal ellipsoids are drawn at 50% probability.

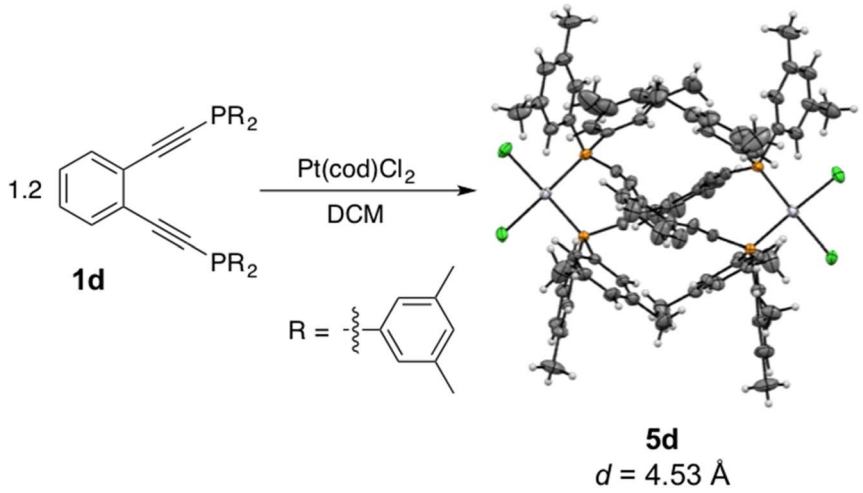

Scheme 3 Synthesis and X-ray crystallographic structure of the Pt(II) phosphine enediyne-bridged dimer **5d**. Thermal ellipsoids are illustrated at 50% probability and the interalkynyl distance (*d*) is provided below.

increased alkyne termini separation. Buchwald reported a similar enediyne-bridged Pd(II) dimer of **1a** on the basis of a saturation transfer experiment and suggested that the dimeric and monomeric Pd(II) complexes of **1a** were in equilibrium with one another.[35,43] Our observations with **5d**, however, do not indicate interconversion between this dinuclear species and the mononuclear complex **3d**, likely due to the slower ligand exchange kinetics observed for platinum complexes relative to their lighter congeners.

The ^{31}P NMR chemical shifts of **3a–3g** show a similar trend to that observed for the free ligands **1a–1g**. There is a large discrepancy (>30 ppm) in the chemical shifts of the aromatic-(**3a–3e**) and aliphatic-substituted (**3f–3g**) metalloenediynes; however, all aryl complexes give ^{31}P NMR resonances within a 3 ppm range. From the chemical shift data alone, the remote substitutions at the *meta* or *para* positions of the phenyl rings at the phosphine termini do not appear to drastically change the chemical environment about the phosphine. However, the rapid degradation of **3a–3b** and **3d** relative to **3c** and **3e** at −20 °C suggests that the aryl substituted metalloenediynes functionalized with electron donating groups are more thermally sensitive than those bearing electron withdrawing groups.

Crystalline material was obtained from vapor diffusion of hexane or pentane into saturated dichloromethane solutions of **3e** and **3f**, respectively, at −20 °C and X-ray crystallographic analysis confirms these complexes as square planar Pt(II) phosphine enediyne dichloride complexes. Deviations from linearity of ∼15° and 7° are observed in the C–C≡C and C≡C–P angles for both **3e** and **3f**; however, these deviations are anticipated as bent acetylenic units are commonly observed for enediyne complexes and have been attributed to in-plane π–π repulsions between the alkyne moieties (Table 3S†).[31] The inter alkyne termini distances are found to be 3.13 and 3.10 Å for **3e** and **3f**, respectively, which are considerably shorter than those computationally predicted for the Pd(II) and Pt(II) analogues of **1a** (3.3 Å).[35] The alkyne termini separation of ligand **1e** is significantly reduced (>1.0 Å) upon platination, clearly demonstrating the drastic structural changes that can accompany metal ion complexation. The interalkynyl distances of **3e** and **3f** are well within the critical distance experimentally proposed by Nicolaou[23] (3.2–3.31 Å) and computationally by Schreiner[25] (2.9–3.4 Å) suggesting that these divalent complexes, and derivatives thereof, should cyclize spontaneously at ambient temperature. It is important to note that the solid-state structures of **3e** and **3f** are quite similar in all bond lengths and angles despite having notably different R-groups at the phosphine termini (**3e**: R = Ph-m_2CF_3; **3f**: R = ^{i}Pr). These data demonstrate that complexation of free ligands **1a–1g** with Pt(II) has generated a suite of metalloenediyne complexes with a nearly uniform, rigidly defined structure. As a result, changes in geometric influences on Bergman cyclization are minimized allowing for clearer interrogation of electronic effects caused by variations in phosphine termini functionalization.

Differential scanning calorimetry has been used to probe the cyclization temperatures of **3a–3g**. Although these metalloenediynes all demonstrate solid-state cyclization, complexes **3a–3d** and **3f–3g** show exothermic maxima between 106–177 °C, while **3e** cyclizes at a considerably higher temperature, 236 °C (Table 1). The cyclization temperatures of aryl-substituted metalloenediynes increase as electron donating substituents are replaced with electron withdrawing groups suggesting that the former are more thermally reactive than the latter. The elevated cyclization temperature of **3e** relative to the other derivatives likely results from solid-state packing differences (*i.e.*, π-stacking between aryl rings, hydrogen bonding with fluorine atoms, *etc.*) not experienced by the other metalloenediynes.

It is challenging to directly compare the cyclization temperatures of **3a–3b** and **3d–3e** to their corresponding free ligands, **1a–1b** and **1d–1e** due to differences in their phases during DSC analysis in which solid-state cyclization temperatures are often upwards of 70 °C higher than those of neat liquids. However, the data clearly show that metalation leads to a drastic reduction in the thermal activation barrier to diradical generation

Table 1 Solid-state Bergman cyclization temperatures of Pt(II) phosphine enediyne dichloride complexes **3a–3g** determined by differential scanning calorimetry

Bergman cyclization temperature/°C		
	Onset	Max
3a	75	116
3b	70	120
3c	110	177
3d	65	106
3e	208	236
3f	100	139
3g	91	140

and suggests that these metalloenediynes should demonstrate facile cycloaromatization under ambient solution conditions. These results are unsurprising as the use of coordination chemistry to geometrically modulate Bergman cyclization has been well established.[35,41,44–51] Moreover, the range of cyclization temperatures across this series of metalloenediynes indicates that electronic substitutions on the ligand framework, while seemingly inert in the free ligands, make dramatic impacts on the electronic component of the cyclization barrier in these well-defined, square geometric complexes.

Electronic modulation of the activation barriers to thermal Bergman cyclization

While solid-state cyclization temperatures and crystallographically-determined inter alkyne termini distances provide an approximation of the thermal reactivity of complexes **3a–3g**, kinetic studies in solution on the cyclization of these metalloenediynes can accurately measure activation barriers to Bergman cyclization and determine rates of cycloaromatization. Comparison of kinetic activation parameters across this series of metalloenediynes reveals the extent to which phosphine functionalization electronically influences thermal Bergman cyclization rate.

To that end, ^{31}P NMR spectroscopy was used to monitor the conversion of metalloenediynes **3a–3g** to their corresponding cyclized products **4a–4g** in the presence of 1,4-CHD in deuterated chloroform (Scheme 4). Though a reliance of cyclization rate on H-atom donor concentration has been observed for benzannelated enediynes, this dependence is less pronounced at high radical quench concentrations.[30,42,52–62] Additionally, analysis of Bergman cyclization kinetics for the original *in situ* cycloaromatization of **1a** with a soluble $PdCl_2$ source found this reaction to be essentially zero order in 1,4-CHD.[35,43] Therefore, only a 100-fold excess of 1,4-CHD was used in this study to establish pseudo-first order conditions. Metalloenediynes **3a–3g** were purified directly before use to ensure the integrity of the samples. All studies were performed in triplicate, under ambient conditions, and in the presence of triphenylphosphine oxide (Ph_3PO) which served as an inert internal standard. The disappearance of **3a–3g** was followed to at least 90% completion by integration of the ^{31}P NMR signal of the starting metalloenediyne *vs.* that of Ph_3PO. Cyclization was monitored in 5 °C increments for each complex: **3b** (5–20 °C); **3a**, **3d** (10–25 °C); **3c** (15, 25–35 °C); **3e–3g** (25–40 °C), and all samples were observed to have well-behaved pseudo-first order kinetics ($R^2 > 0.98$) at all temperatures (Fig. 2S†). These data were then used to determine rate constants and derive the free energy of activation ($\Delta G^{\ddagger}$) for this radical-mediated transformation.

By ^{31}P NMR spectroscopy, the cyclization of all complexes except **3g** proceeds cleanly to the corresponding cyclized product in >90% yield (Fig. 2). In the case of **3g**, though the cyclized product **4g** is identifiable by ^{31}P NMR, other phosphorus-containing species are also observed suggesting that self-quenching of the diradical intermediate with internal C–H bonds from the cyclohexyl substituents may occur leading to the formation of multiple products. Following the kinetics measurement, the reaction mixtures from all trials for a given compound were combined and purified using preparatory silica gel chromatography allowing for isolation and characterization of the cyclized compounds **4a–4f**. Unfortunately, attempts to isolate **4g** *via* this same purification method proved

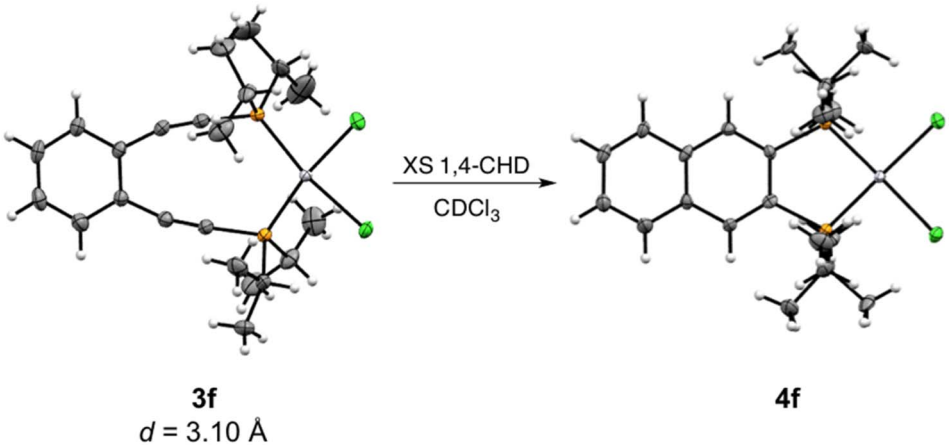

Scheme 4 Ambient temperature Bergman cyclization of **3f** to generate **4f**. Thermal ellipsoids are illustrated at 50% probability and the inter-alkynyl distance (*d*) is given below.

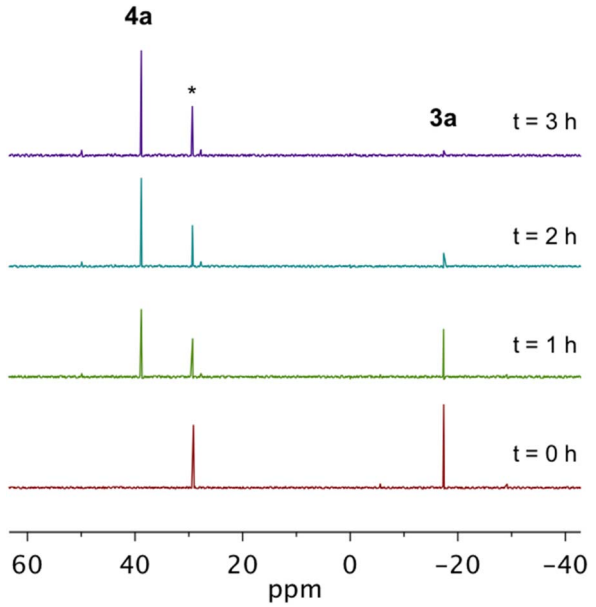

Fig. 2 ^{31}P NMR spectroscopy demonstrating the cyclization of **3a** (δ = −17.44 ppm) in the presence of 1,4-CHD to afford **4a** (δ = 39.42 ppm) in near quantitative yield at 25 °C. These data are representative of the cyclizations of **3b–3f** which proceed cleanly to the cyclized products **4b–4f**. The designated (*) signal corresponds to triphenylphosphine oxide, the internal standard.

unsuccessful due to the high quantities of side products. Complexes **4a** and **4c–4f** were isolated as crystalline materials and X-ray crystallography shows that these Bergman cyclized products adopt nearly idealized square planar geometries about the divalent platinum center (Fig. 3S†). The Pt–P and Pt–Cl bond lengths are conserved across the series and are consistent with other Pt(II) phosphine dihalide complexes (Table 4S†).[41,63] Comparison of **4e** and **4f** to their metalloenediyne counterparts **3e** and **3f** shows slight bond angle changes, the most notable being the P1–Pt1–P2 angle which is reduced ∼17° upon closing of the inter alkyne termini distance.

Analysis of the room temperature kinetic studies reveals that the rate of Bergman cyclization of these Pt(II) metalloenediynes increases on the order of **3f** < **3e** < **3g** < **3c** < **3a** ∼ **3d** < **3b** (Fig. 3a–b). In fact, cyclization of **3b** proceeds so rapidly at room temperature that an accurate assessment of the rate could not be made. Consequently, cyclization studies had to be performed at or below 20 °C to obtain reliable kinetic data which could then be extrapolated to gain insights into the reactivity of this complex at 25 °C. Similarly, complexes **3a** and **3d** show rapid cycloaromatization at room temperature requiring all subsequent kinetic studies to be performed at low temperature.

At 25 °C, the half-life ($t_{1/2}$) of cyclization for **3a–3g** spans a range of almost 35 hours, highlighting the dramatic thermal tunability that is afforded through functionalization of the phosphine enediyne with various electron donating and withdrawing substituents (Table 2). The temperature-dependent cyclization rates allow for the generation of Eyring plots and the elucidation of the free energy of activation, $\Delta G^{\ddagger}$, at room temperature (Fig. 3c, d and 4S†). Cyclization parameters have been experimentally determined for both aryl (**3a–3e**) and aliphatic (**3f–3g**) substituents and in nearly all cases, the aliphatic substituents show slower cyclization kinetics and higher activation barriers to cycloaromatization than their aryl counterparts (Table 2). For acyclic enediynes, Schreiner has shown that direct functionalization of the alkyne termini with alkyl groups increases the endothermicity of Bergman cyclization due to stabilization of the enediyne core orbitals.[25] We observe a similar increase in endothermicity upon alkyl substitution at the phosphine termini; however competing internal C–H bond quenching of the diradical intermediate in **3g** suggests that the rate-determining pathway for the alkyl substituent constructs may differ from the mechanistic consistency of the aryl family.

With regards to the aryl phosphines (**3a–3e**), the presence of electron donating substituents (**3b** and **3d**) clearly accelerates Bergman cyclization while electron withdrawing groups (**3c** and **3e**) retard cyclization. In some cases, the rate enhancement for structurally analogous metalloenediynes is minimal and in others, it is quite dramatic. For example, complex **3b** (R = Ph-*p*OCH_3) cyclizes approximately 10× faster than **3c** (R = Ph-*p*CF_3) whereas **3d** (R = Ph-*m*$_2CH_3$) has a cyclization rate >30 times faster than the analogous **3e** (R = Ph-*m*$_2CF_3$). As expected, these trends are mirrored in the $\Delta G^{\ddagger}$ data, with the activation barrier varying by ∼2.6 kcal mol^{-1} across the series of aryl-substituted metalloenediynes (Table 2). Specifically, for the *para*- (**3b** and **3c**) and *meta*-substituted (**3d** and **3e**) derivatives, the free energy of activation decreases by ∼1.4 and ∼2.2 kcal mol^{-1}, respectively, when electron withdrawing –CF_3 groups are replaced with electron donating substituents. Overall, these data clearly highlight the role that electronic substitutions can play in controlling activation barriers to Bergman cyclization.

Probing the origin and mechanism of electronic control for aryl-substituted metalloenediynes

The rate dependence for Bergman cyclization on electron donating and withdrawing substituents for acyclic enediynes has been established by Schmittel[33] and Schreiner.[34] Here, as electron withdrawing substituents are added at the alkyne termini positions, the activation barrier for the reaction decreases due to reduced electron–electron repulsion of the in-plane pπ-orbitals in the transition state which facilitates C–C bond formation. This result is intuitive in that distributing electron density across multiple atoms *via* electron withdrawing functionalities decreases charge repulsion, whereas electron donors increase it.

Broadly, our results are consistent with this literature precedence. Complexes with categorical electron withdrawing aryl substituents (**3a–3e**) generally have shorter half-lives and lower activation barriers to cycloaromatization than do those with electron donating alkyl substituents (**3f** and **3g**) (Table 2). However, the rate enhancement within the series of the aryl-substituted metalloenediynes with electron donating groups (**3b** and **3d**) relative to those with electron withdrawing groups (**3c** and **3e**) is counter to this paradigm. The additional complexity of **3a–3e**, *i.e.*, the presence of an insulating

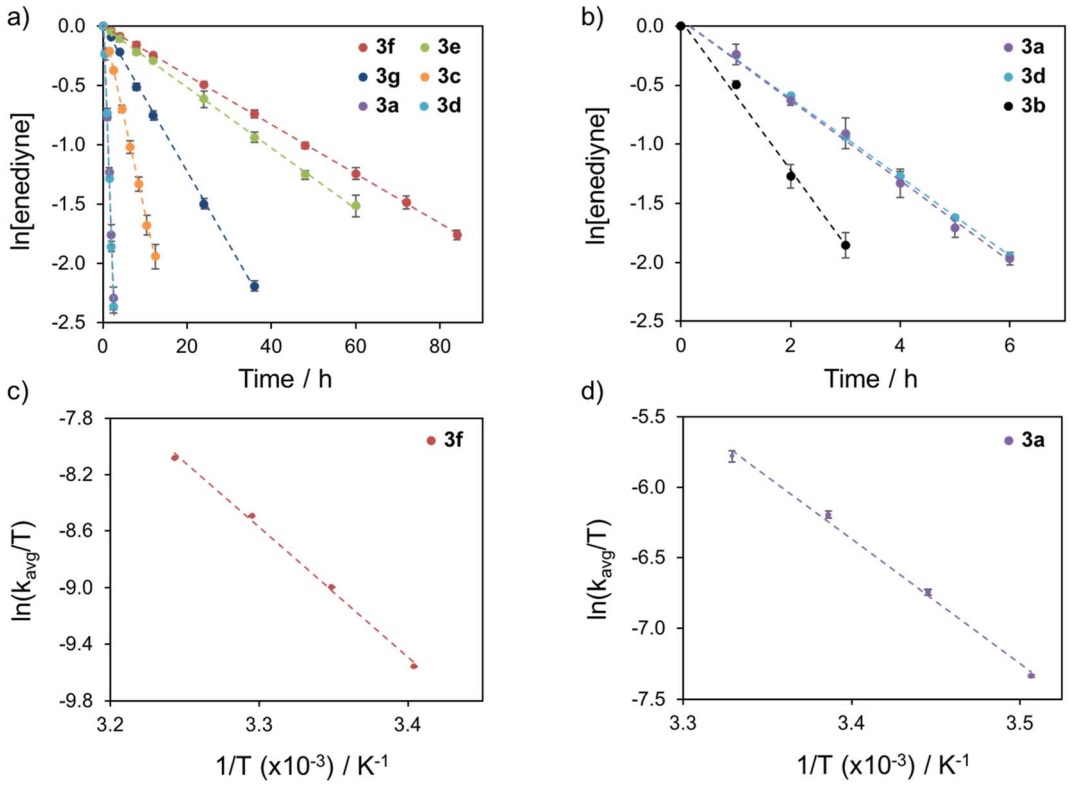

Fig. 3 Summary of Bergman cyclization kinetics for complexes **3a–3g** (a) at 25 °C and (b) at 15 °C. Sample Eyring plots of (c) **3f** and (d) **3a** used to calculate activation parameters.

Table 2 Kinetic activation parameters for the thermal Bergman cyclization of complexes **3a–3e** (aryl) and **3f–3g** (alkyl) at 25 °C. Functionalization of aromatic rings with electron donating (**3b**, **3d**) and electron withdrawing groups (**3c**, **3e**) leads to acceleration and retardation of cyclization kinetics, respectively[b]

Experimental kinetic activation parameters at 25 °C kcal^{-1} mol^{-1}				
Compound		$t_{1/2}$/h	k/h^{-1}	$\Delta G^{\ddagger}$
●	**3f**	33.3	0.02	19.72
●	**3e**	27.1	0.03	19.62
●	**3g**	11.3	0.06	19.10
●	**3c**[a]	4.4	0.16	18.45
●	**3a**	0.73	0.95	17.47
●	**3d**	0.70	0.99	17.47
●	**3b**	(0.36)	(1.90)	17.07

[a] Complex **3c** contained ~5% Pt(cod)Cl$_2$ impurity. [b] Data in ( ) extrapolated from Eyring plot.

heteroatom (P) and a PtCl$_2$ fragment, diversify the electronic structures of these constructs globally, and within the geometrically equivalent metalloenediyne frameworks. This invariance is supported by the X-ray structures of Bergman cyclized Pt(II) products **4a** and **4c–4e** (*vida supra*) suggesting that there exists minimal geometric differences amongst these complexes. Thus, an important feature of this molecular suite is that we have in essence, independently accounted for the geometric and electronic contributions to thermal Bergman cyclization, which can be readily evaluated using computational methods.

The reaction profiles of simple organic enediynes[25,31,34,64] and metalloenediynes[37,65–67] to the diradical intermediate have been successfully modeled with density functional theory (DFT) and yield activation barriers consistent with experimental findings. The choice of theoretical approach plays a key role in modeling transition state structures and predicting activation energies. Many have noted that hybrid Hartree–Fock DFT methods such as B3LYP do not effectively model the diradical intermediate leading to spurious results, which at times can overestimate barrier heights by upwards of 8 kcal mol^{-1}.[25,31,68,69] It has been demonstrated however, that pure density functionals such as BLYP and BPW91 give computational activation parameters that are consistent with those obtained experimentally.[34,37]

Bergman cyclization of **3a–3e** was modeled with DFT using Gaussian 16 (ref. 70) to confirm the geometric similarities across this suite of metalloenediynes, obtain activation parameters, and to visualize the molecular orbitals that play key roles in the formation of the reactive diradical intermediate. Both B3LYP[71–73] and B3PW91 [72] yielded activation barriers that were consistently 5–10 kcal mol^{-1} higher in energy than those obtained experimentally, even when correcting for empirical dispersion *via* Grimme's GD3BJ[74] damping function. The results from the pure BPW91 [71,75–79] functional however, were consistent

with experimental findings within <2 kcal mol^{-1}. Therefore, all structures were optimized using the (U)BPW91 functional with the 6-31G** basis set and the LANL2DZ[80–82] pseudopotential was applied to transition metal atoms. The spin-unrestricted approach[83] was used to compute diradical intermediates which were found to be open-shell singlet in character. Vibrational frequency calculations were performed at the (U)BPW91/6-31G**/LANL2DZ level of theory to confirm convergence to minima for ground state geometries and first-order saddle points for transition state structures, respectively, as well as provided zero-point energy (ZPE) corrections at room temperature. After performing all calculations in the gas phase, solvated single point energies were evaluated using the PCM model[84–88] at the same level of theory to account for energy differences due to solvation in chloroform ($\varepsilon = 4.71$).

Bergman cyclization reactions encounter multiple transition states: the first involves conversion of the enediyne to the diradical intermediate while subsequent barriers describe the H-atom abstraction steps to yield the benzannelated product. Relative to parent (*Z*)-hex-3-ene-1,5-diyl frameworks, incorporation of the enediyne backbone into an aromatic ring is known to increase the endothermicity of diradical formation while concomitantly lowering the barrier to retro-Bergman ring opening due to reduced aromatic stability of the naphthyl product.[30,42,53,54,57–60] As such, the rate of cyclization of benzannelated enediyne complexes depends not only on formation of the diradical intermediate (k_1) but also on the retrocyclization (k_{-1}), while the H-atom abstraction (k_2) pathways are considered comparable for structurally analogous compounds. However, when pseudo-first order conditions are achieved using sufficiently high concentrations of radical quenching agent, cyclization becomes the rate-limiting step.[60,61]

The interplay between k_1 and k_{-1} on the observed rate can be gleaned from the computational barrier heights for the forward and retrocyclization reactions. Here, for the fastest cyclizing compound **3b**, the forward barrier height is one of the lowest of the set **3a–3e** by 1.8 kcal mol^{-1}, while the barrier to retrocyclization is the highest by 1.2 kcal mol^{-1}, therefore contributing to the largest observed rate. Conversely, **3e** has the most significant barrier to Bergman cyclization and the smallest to retrocyclization, thereby retarding the observed reaction rate appreciably. Thus, the two barriers have complementary effects on the rate of the overall cyclization reaction. The first activation barrier leading to formation of the reactive diradical intermediate, however, is the more energetically dominant of the two contributors to the overall rate constant for these Bergman cyclization reactions.

These variations in state energies and rates must derive from geometric and/or electronic structural changes at the molecular level.[56] Comparison of the computed structures for the metalloenediynes **3a–3e** finds that all compounds have nearly identical enediyne core geometries, to within ~0.05 Å and 3° in bond lengths and angles, respectively. Furthermore, the transition state geometries, **3a-TS–3e-TS**, are also consistent in bond and angle metrics between all complexes investigated (Fig. 4). These computational findings agree with the experimental crystallographic data and support the proposal that the observed rate enhancements or retardations result from electronic rather than structural differences that manifest upon R-group modification at the phosphine termini. For complexes **3a–3e**, geometric rearrangements between the reactants and products are minimal due to the structure enforced by the square planar metal center. Consequently, electronic reorganization may exhibit a greater level of control over the cyclization event than what has been observed previously in simple enediyne systems.

For enediyne frameworks, electron repulsion between filled in-plane π-orbitals accounts for considerable destabilization upon bending of the alkynes to facilitate sigma C–C bond formation.[56] Removal of electron density from this in-plane π-system promotes formation of the cycloaromatized products by lowering the energy of the transition state. The relationship between ^{13}C NMR chemical shifts and atomic charges has been studied both experimentally and computationally. Although effects may vary depending on hybridization, the general consensus is that for a series of closely related compounds, charge-shift trends can provide a good approximation of electronic polarization.[89–92] Specifically, ^{13}C NMR spectroscopy has been shown to be a sensitive reporter of electron density in acetylenic moieties, with a correlation demonstrated between the shielding of an alkyne carbon and the π-electron density on that atom.[93–98] The distribution of electron density in the alkyne carbons of a ground state structure has important consequences on the electronic rearrangement that occurs upon formation of the reactive diradical intermediate. Much like crystallographic analysis, ^{13}C NMR investigations of the reactive metalloenediyne complexes **3a–3e** were prohibited due to the long acquisition times needed for data collection and the highly reactive nature of the complexes. However, with computational support that structural differences amongst **3a–3e** are minute, the geometrically-locked phosphine oxide free enediyne ligands, **2a–2e**, can be used as model systems to experimentally interrogate alkyne charge distribution in the ground state.

It is clear from the ^{13}C NMR shifts of **2a–2e** that the alkyne carbon adjacent to the phosphine atom, C_A, supports considerably more electron density than the alkyne carbon closer to the benzannelated backbone, C_B (Fig. 5). The degree of shielding (C_A) and deshielding (C_B) of these signals reveals that all phosphine oxide ligands, regardless of aryl ring R-group substitution, are polar in nature, with the dipole moment situated such that C_A is more electron-rich than C_B. However, there appears to be a correlation between the identity of the R-group and the magnitude of alkyne polarization, with ligands bearing electron withdrawing substituents being more highly polarized than those supporting electron donating substituents ($\Delta\delta$(C≡C): **2e** = 19.6 ppm; **2b** = 12.6 ppm). The polar nature of the alkyne carbons of the free ligand phosphine oxides demonstrates that subtle changes in the enediyne framework itself can be used to tune the electronic properties of ligand. Moreover, it suggests that there likely exist differential charges in the acetylenic moieties of the reactive metalloenediyne complexes **3a–3e** that, over the course of the cyclization reaction, may play a role in governing barrier heights to diradical formation. This ^{13}C NMR charge-shift analysis may not be indiscriminately applied to all acetylenic systems; however,

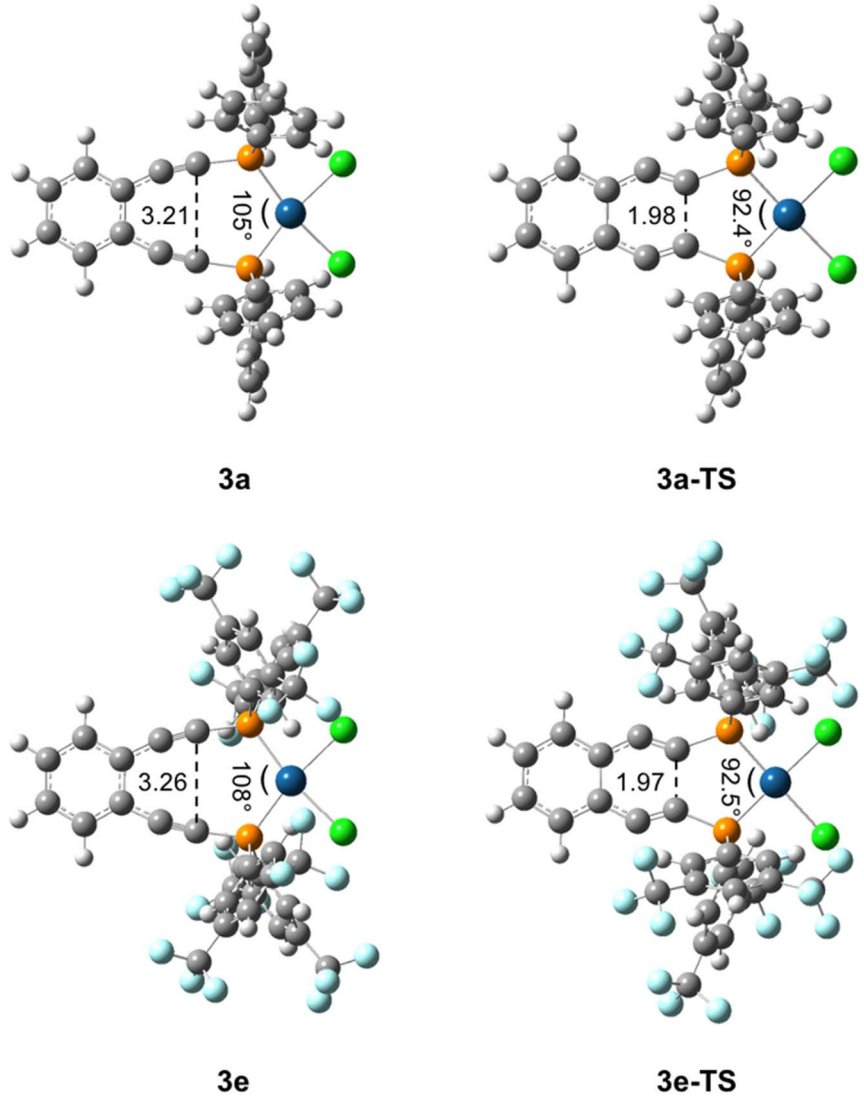

Fig. 4 Key structural parameters of (U)BPW91/6-31G**/LANL2DZ optimized metalloenediynes **3a** and **3e** and their transition states **3a-TS** and **3e-TS**. These bond length (Å) and angle (°) changes are representative of those observed for all metalloenediynes **3a–3e** and transition states **3a-TS–3e-TS**.

correlations can be drawn in this case due to the highly conserved geometry across the series of phosphine oxide enediyne ligands and corresponding metalloenediynes.

Although ^{13}C NMR spectroscopy provides information about the relative distribution of electron density in the alkyne carbons of the organic-only enediyne oxide frameworks, in-depth charge analysis of the computed ground state (GS) and transition state (TS) structures of the reactive metalloenediynes **3a–3e** can more definitively establish whether there exists a correlation between the polarization of the enediyne framework and activation barriers to Bergman cyclization. Nuclear rearrangement (*i.e.*, bending of the alkynes) necessitates concomitant electronic reorganization to both facilitate σ-bond formation and to promote development of the diradical intermediate. Despite the importance of C_A in C–C bond formation, consideration of only these differential charges may be an oversimplification of the electronic parameters that govern barriers to thermal Bergman cyclization. Indeed C_B, though not directly involved in bond formation, is the site of diradical generation, and as such, likely experiences electronic perturbations which may also modulate activation barriers to cycloaromatization.

Bearing this in mind, natural bond order (NBO) charges from the computed GS structures of **3a–3e** and those of corresponding transition states, **3a-TS–3e-TS**, can be used to calculate the dipole moment of each alkyne (C_A–C_B) according to eqn (1) (Fig. 6a). In this case, the magnitude of the dipole, $\vec{\mu}$, is given by the product of the differential charges of the alkyne carbons ($q_A - q_B$) and the separation between those charges, r_{AB}. It is important to consider not only the polarization of a single acetylenic unit but also the dipole interaction energy which is operative as geometric rearrangement brings the two arms of the enediyne framework in close proximity to initiate C–C bond formation. Eqn (2) shows that the dipole interaction energy is

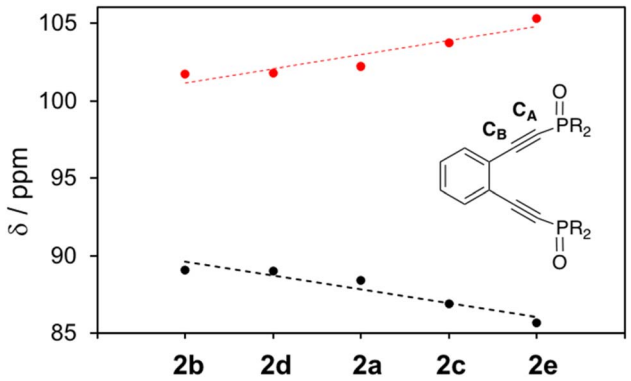

Fig. 5 ^{13}C NMR resonances of phosphine oxide analogues **2a–2e** revealing the polar nature of the alkyne carbons, C_A (black) and C_B (red), the magnitude of which is enhanced in the presence of electron withdrawing substituents.

dependent on the dipole moments, $\vec{\mu}_1$ and $\vec{\mu}_2$, of the alkyne fragments, the separation between the center of the two dipoles, r_{12}, the permittivity of free space, ε_o, and the projection of the dipoles on one another, θ_1, θ_2, and θ_{12} (Fig. 6b). It is clear from the structures of **3a–3e** and **3a-TS–3e-TS** and the orientation of the C_A–C_B dipoles that there are both attractive and repulsive interactions between the two opposing alkynes; undoubtedly, the magnitude of these coulombic forces influences the electronic contributions to the activation energy for the reaction.

$$\vec{\mu} = (q_A - q_B)(r_{AB}) \quad (1)$$

$$E = \frac{-\vec{\mu}_1 \vec{\mu}_2}{4\pi\varepsilon_o {r_{12}}^3}(\cos\theta_{12} - 3\cos\theta_1 \cos\theta_2) \quad (2)$$

For all complexes in the ground state, C_A and C_B are negatively and positively polarized, respectively, resulting in a net dipole moment in the direction of C_A (Fig. 7a). The magnitude of this C_A–C_B dipole increases in the presence of electron withdrawing substituents such that complexes **3c** and **3e** show the greatest charge separation between the alkyne carbons, consistent with the data from the ^{13}C NMR analysis of the phosphine oxide enediyne ligands **2a–2e**. Comparison of the ground state dipole interaction energies to the experimentally determined barrier height reveals an empirical correlation between the free energy of activation and the R-group of the phosphine-bound aryl rings (Fig. 7b). The complex with the highest activation barrier (**3e**: R = Ph-m_2CF_3) has the greatest coulombic repulsion between the alkyne fragments while the complex with the most facile cycloaromatization (**3b**: R = Ph-pOCH$_3$) has the smallest dipole interaction energy.

NBO charge analysis of the computed transition state structures (**3a-TS–3e-TS**) shows that as geometric rearrangement begins, electron density flows from C_B towards the site of σ-bond formation resulting in an increased negative charge on C_A (Fig. 7a). The dipole moment (C_A–C_B) in the transition state lies in the same direction as that of the ground state and an overall increase in the polarization of the alkyne carbons is observed. Plotting the experimental activation barriers as

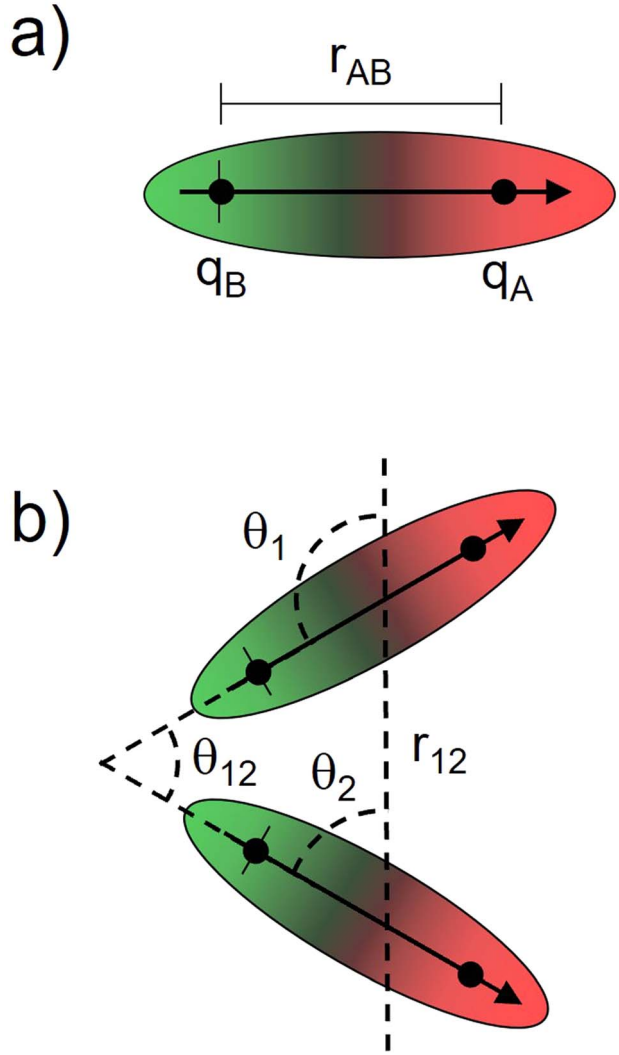

Fig. 6 Global distribution of charge throughout the enediyne framework can be approximated by considering (a) the net polarization of alkyne carbons C_A and C_B and (b) the magnitude of coulombic interactions between opposing acetylenic dipoles.

a function of TS dipole interaction energy reveals the same correlation between enediyne R-group and free energy of activation as was observed with the GS structures (Fig. 7c). For complexes **3a-TS–3e-TS**, those with electron withdrawing substituents are overall more polar in the transition state than those with electron donating groups. This NBO charge analysis provides a global picture of electron distribution within the enediyne framework and indicates that the presence of electron withdrawing substituents on the terminal phosphine aryl rings increases the coulombic repulsions in the transition state between the two acetylenic moieties in these metalloenediynes leading to an increase in barrier height for Bergman cyclization.

In addition to the dipole–dipole interaction energy contributions to the barrier, interrogation of the frontier molecular orbitals (FMO) of the enediyne core may give a more detailed perspective on how the distribution of electron density across the acetylenic carbons as a function of R-group influences the

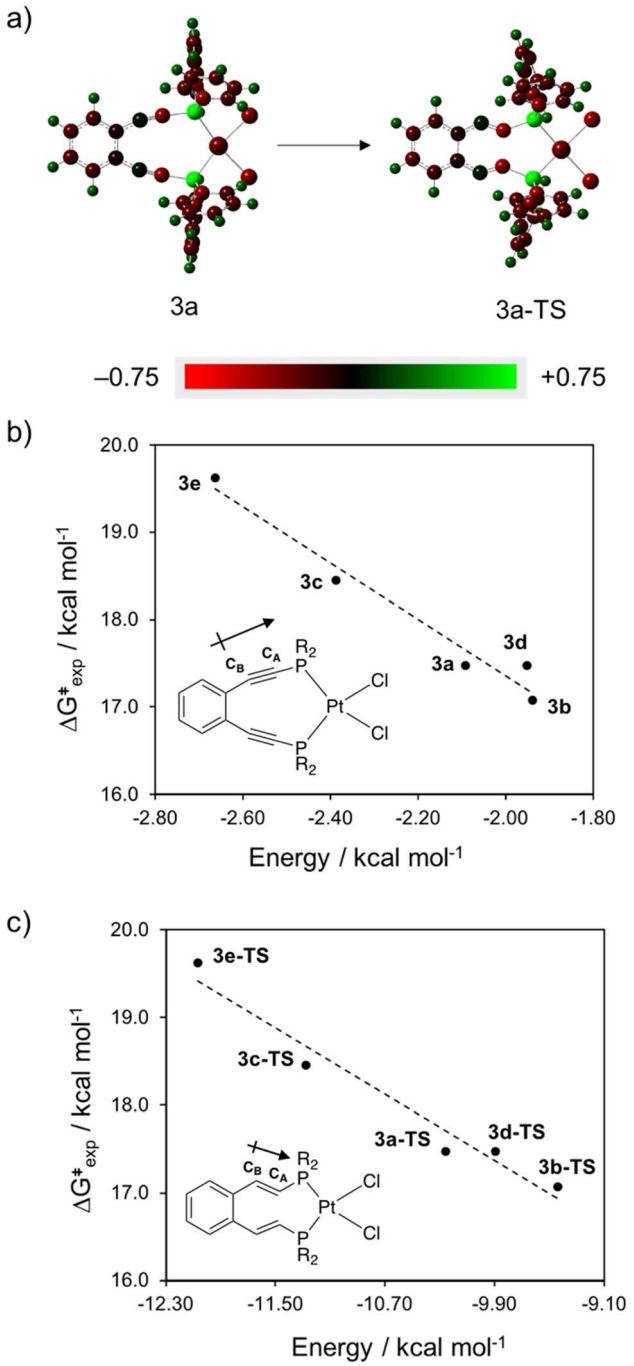

Fig. 7 Plots of $\Delta G^{\ddagger}$ as a function of alkyne dipole interaction energy, evaluated using (a) NBO charge analysis (representative example of **3a** shown) for (b) enediyne ground states (**3a–3e**) and (c) calculated transition states (**3a-TS–3e-TS**) demonstrating the relationship between alkyne polarity (C_A–C_B) and experimental barrier height to thermal Bergman cyclization.

energetics for the cycloaromatization reaction. For the representative cyclization reaction involving (*Z*)-enediynes, Alabugin has computationally shown destabilization of the out-of-phase combination of the in-plane π-orbitals to be the largest energetic penalty paid to reach the transition state and achieve *p*-benzyne formation. This destabilizing effect, however, is offset by stabilization of the in-phase, in-plane π-orbitals which contribute to the formation of the new carbon–carbon sigma bond.[56,69] A minor, secondary source of stabilization comes from the out-of-plane alkyne π-system which yields a conjugated aromatic product upon H-atom abstraction.[56] Since the activation barrier to Bergman cyclization is simply the difference between the energies of the reactants and the transition state,[69] the degree of stabilization or destabilization of the in-plane symmetric and antisymmetric π-orbitals, respectively, should predominantly govern the barrier height and thus thermal cycloaromatization of enediyne-containing constructs.

Examination of the molecular orbital manifolds of **3a–3e** and their associated transition states reveals several orbitals with in-plane π-orbital density indicating that it is an orbital ensemble rather than a singular stabilization/destabilization effect that contributes to the overall acceleration or retardation of Bergman cyclization kinetics. Regardless, some of these in-plane π-orbitals show markedly greater energy differences between the ground and transition states suggesting that they contribute significantly to the overall barrier height. The antisymmetric in-plane π-orbitals, which become the site of diradical formation, are destabilized in the transition state for all complexes **3a–3e**. For a set of complimentary orbitals in the ground state, electron density is delocalized across the in-plane π-system as well as the platinum center and the two chloride ligands. In the transition state however, the electron density of these orbitals is now almost exclusively localized in the in-plane π*-orbitals. The magnitude of this destabilization varies as a function of R-group, with complexes bearing electron withdrawing groups, **3e**, being destabilized to a greater extent than those with electron donating substituents, **3b** (Fig. 8). When viewed collectively with the NBO charge analysis, this electronic reorganization in the transition state results in differentially increased electron–electron repulsions between the approaching acetylenic carbons.

While this destabilization of the antisymmetric in-plane π-orbital is significant for all complexes **3a–3e**, it is offset by the stabilization of the symmetric in-plane π-orbitals. Within this orbital manifold, complexes with electron withdrawing substituents generally have a distribution of orbitals with similar character compared to those with electron donating substituents, where electron density is localized to a single orbital. This aggregation of orbitals makes pinpointing the stabilization effect to a single orbital challenging. Nevertheless, comparison of a set of complimentary in-phase π-orbitals for complexes **3b** and **3e** finds the ground state orbitals to be similar in character to those of the antisymmetric set, with electron density distributed predominantly within the square planar core of the metalloenediyne. In the transition state, electron density about the $PtCl_2$ fragment has decreased and there remains overlap between the in-phase alkyne π-orbitals, although the magnitude of this interaction appears R-group dependent (Fig. 8). In general, complexes with electron donating groups on the aryl phosphine rings have substantially greater stabilization of these in-phase, in-plane π-orbitals compared to those complexes bearing electron withdrawing substituents. This is consistent with the NBO charge analysis

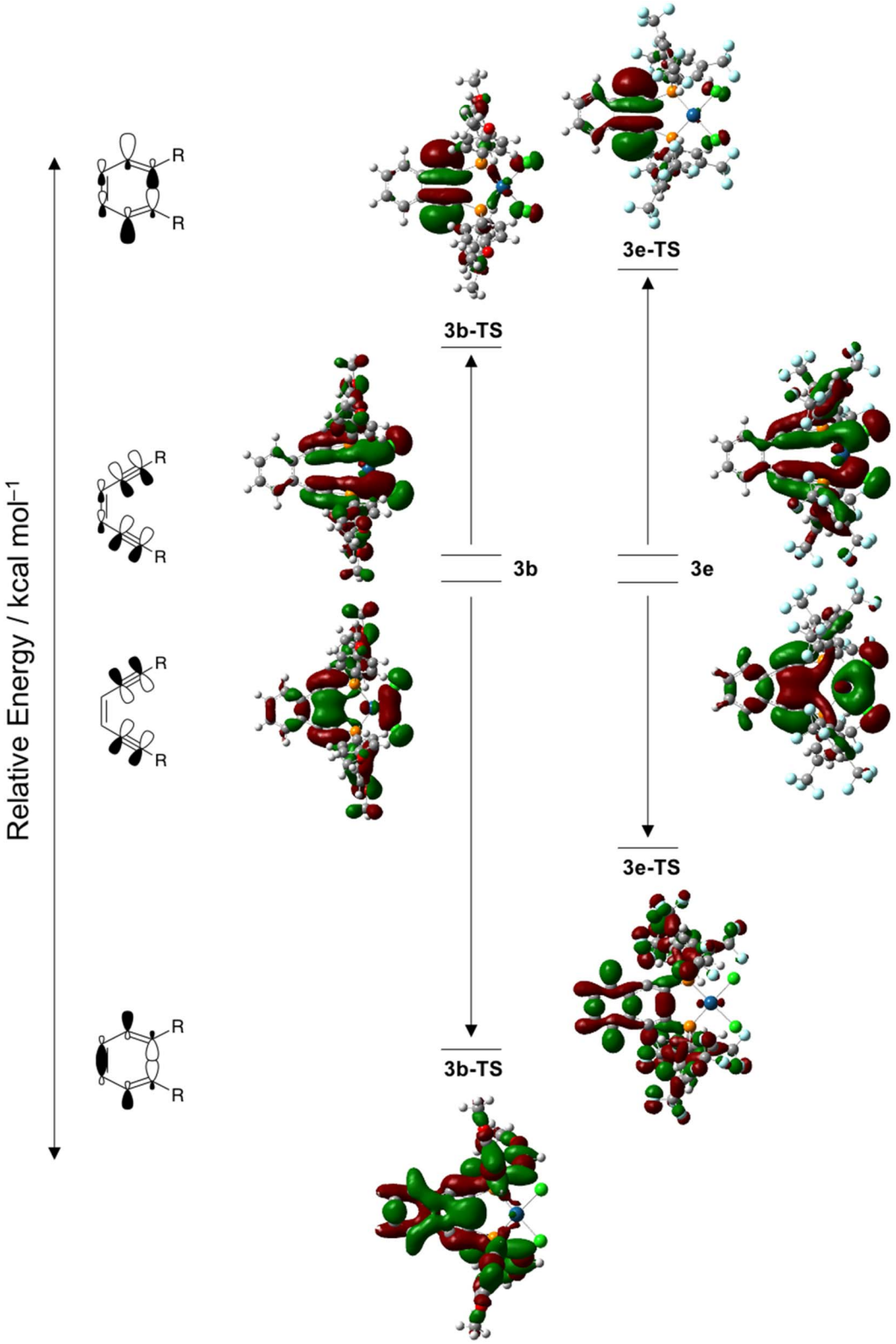

Fig. 8 Walsh diagram showing the in-plane alkyne π/π^*-orbitals most stabilized and destabilized by the cyclization reaction of complexes **3b** and **3e** and their associated transition states **3b-TS** and **3e-TS**. The degree of stabilization or destabilization of these orbitals in the transition state varies significantly due to the presence of electron donating (**3b**: R = Ph-*p*OCH_3) or electron withdrawing (**3e**: R = Ph-m_2CF_3) groups at the alkyne termini.

which finds complexes with less polar acetylenic bonds have lower barriers to cycloaromatization.

An additional noteworthy point: the symmetric in-plane π-FMOs for **3a-TS**, **3b-TS**, and **3d-TS** have considerably more electron density within the aryl ring system which are predominately pσ-character, than do the corresponding orbitals of **3c-TS** and **3e-TS**, mainly pπ- and $-CF_3$ lone pair character. The orbital parentage for complexes with electron donating substituents suggests that there exists π-orbital mixing between the acetylenic orbitals and the aryl ring system which substantially lowers the energy of the transition state orbitals involved in the formation of the developing C–C bond. Since the aryl ring system is chiefly low-lying pσ-character, this π-orbital mixing is reflected in a net stabilization of the transition state which affords a lower activation barrier to Bergman cyclization. The presence of electron withdrawing substituents on the terminal aryl rings decreases the energy of these pσ-orbitals such that they are no longer capable of interacting with those of the enediyne core. Consequently, only minimal stabilization of the developing σ-bond occurs which results in an overall increase in the activation barrier to cycloaromatization.

Finally, the degree with which the alkyne pσ- and pπ-density mixes with that of the $PtCl_2$ fragment cannot be ignored. DSC data, experimental cyclization kinetics, and crystallographic analysis (*vida supra*) confirm that the significant rate enhancement or retardation of Bergman cyclization with the aryl-substituted enediynes is electronic in nature and not operable until platination occurs. In general, metalloenediynes with electron donating groups at the *para* or *meta* positions of the aryl rings have a higher percentage of frontier molecular orbitals that show mixing of the $PtCl_2$ fragment with the alkyne orbitals relative to the complexes with electron withdrawing groups in these remote positions. The increased mixing of the alkyne and $PtCl_2$ orbitals stabilizes the transition state which facilitates rapid Bergman cyclization at ambient temperature. Overall, for this suite of reactive metalloenediyne complexes, it appears that the R-group strongly influences the orbital mixing between the enediyne backbone, aryl ring system, and $PtCl_2$ fragment which either promotes (EDGs) or impedes (EWGs) C–C bond formation which is directly reflected in the overall barrier height due to stabilization or destabilization of the transition state, respectively.

Conclusions

The original paradigms illustrating the critical distance for spontaneous Bergman cyclization by Nicolaou (d ~3.2–3.3 Å), and significant geometric rate acceleration using square planar Pt(II) by Buchwald, have stood for more than a quarter century. Our development of a suite of functionalized phosphine enediynes bearing either aliphatic (^{i}Pr, Cy, ^{t}Bu) or aromatic (Ph, Ph-pOCH$_3$, Ph-pCF$_3$, Ph-m_2CH$_3$, Ph-m_2CF$_3$) substituents with donor/acceptor functionality has moved the frontiers of both of these benchmarks simultaneously. With these ligands, we have synthesized a series of cisplatin-like complexes featuring an array of phosphine enediynes that represent the first divalent platinum phosphine enediyne complexes isolated as discrete structures to date. X-ray crystallography indicates that these Pt(II) dichloride complexes have greatly reduced inter alkyne termini distances relative to the free ligands, suggesting that these metalloenediynes should demonstrate very rapid Bergman cyclization under modest conditions. While these structures are primed to cyclize at 25 °C, their half-lives vary considerably ($t_{1/2}$ ~0.6–35 h) depending upon the donating or withdrawing nature of the substituents, even though experimentally, they are structurally analogous.

The geometries and activation parameters of the aryl-substituted complexes are computationally consistent with the experimental findings suggesting that the electronic functionalization is the driving force controlling the cyclization rates and thus the stabilization of this otherwise geometrically reactive framework. The origin of this modulation derives from two coincident phenomena: (1) NBO charge analysis reveals that differential charges between the alkyne carbons contribute to an overall polarization of the in-plane π-system which either promotes (EDGs) or inhibits (EWGs) cycloaromatization and (2) complexes with electron donating substituents experience substantial orbital mixing between the acetylenic π-orbitals, the phosphine-bound aryl ring system, and the $PtCl_2$ fragment resulting in a significant stabilization of the developing σ-bond and transition state. This, concomitant with reduced polarization of the alkyne carbons, lowers the activation barrier dramatically relative to those complexes bearing EWGs where orbital energies are disparate, and mixing is unfavorable. Together these new parameters push the boundaries of enediyne reactivity space well beyond what was originally deemed possible, and thus encourage creative structural manipulations to further advance the reaches of diradical utility.

Materials and methods

Materials

Reactions to synthesize enediyne ligands and platinum(II) phosphine enediyne dichloride complexes were carried out using standard dry box and Schlenk techniques under inert nitrogen atmosphere. All chemicals and solvents were purchased from commercial sources and used as received. Solvents were dried and distilled according to standard protocols unless otherwise noted. Deuterated solvents were dried over 4 Å molecular sieves and used without further purification. Flash and preparative chromatography were performed on silica gel (Sorbtech, 60 Å porosity, 230 × 400 mesh) and (Analtech, 1000 μm), respectively.

Physical measurements

NMR spectra were collected on a Varian Inova 400 or 500 MHz NMR spectrometer using the residual proton resonance of the solvent as an internal reference. All ^{31}P and ^{19}F NMR spectra were externally referenced using 85% H_3PO_4 and 100% trifluoroacetic acid standards, respectively. Mass spectrometry data were acquired on an Agilent 1200 HPLC-6130 MSD mass spectrometer. Differential scanning calorimetry (DSC) measurements were made on a TGA Q10 DSC system with a TA

Instruments thermal analyzer at a heating rate of 10 °C min^{-1}. Infrared spectra were measured on a Nicolet 6700 FT-IR spectrometer equipped with OMNIC software. Elemental analyses were obtained from Robertson Microlit Laboratories, Inc. X-ray crystallographic data were obtained by the Indiana University Molecular Structure Center on a Bruker APEX II Kappa Duo diffractometer using Mo Kα radiation (graphite monochromator). Summaries of X-ray crystallographic analyses can be found in the ESI.†

Computational methods

All calculations were carried out using Density Functional Theory (DFT) as implemented in Gaussian 16.[70] Geometry optimizations were performed with the (U)BPW91 functional and 6-31G** basis set for all structures.[71,75–79] The LANL2DZ effective core potential was used to model transition metal atoms.[80–82] Calculation of the open-shell, diradical intermediates used the broken-symmetry, broken-spin approach which allows for the α and β electrons to be localized on separate carbon centers.[99] Vibrational frequency calculations were performed at the (U)BPW91/6-31G**/LANL2DZ level of theory to confirm proper convergence to minima and maxima for equilibrium and transition state geometries, respectively, and to derive zero-point energy (ZPE) and entropy corrections at room temperature (298.15 K). Single point energy calculations in chloroform (dielectric constant $\varepsilon = 4.71$) were performed using the PCM model[84–88] at the same level of theory to account for energetic contributions from solvation. The energy components were calculated following the standard protocol.[67] Isosurface contour plots of all molecular orbitals were created with Gaussview 6.1.1 with isovalues at 0.02. Coordinates for all optimized geometries can be found in the ESI.†

Synthesis of phosphine enediyne ligands (1a–1h). The TMS-protected precursor enediyne 1,2-bis((trimethylsilyl)ethynyl) benzene, EDTMS, was synthesized according to a published literature procedure[35] and used in all syntheses.

*1,2-Bis((diphenylphosphino)ethynyl)benzene, dppeb (**1a**).* This enediyne has been synthesized using a modified literature procedure[35,43] to yield the ligand as a solid rather than an oil as previously reported. To a solution of EDTMS (2.17 g, 8.00 mmol) in 150 mL THF at 0 °C was added 1.6 M *n*-BuLi in hexanes (10.50 mL, 16.81 mmol) and the reaction mixture allowed to warm slowly to 55 °C. The reaction mixture was stirred at elevated temperature during which time the clear, dark brown solution lightened considerably and became milky. After 3 h, the solution was cooled to 0 °C and chlorodiphenylphosphine (3.16 mL, 17.61 mmol) was added *via* syringe. The mixture was slowly warmed to RT and allowed to stir for 3 h resulting in a clear, dark brown solution. The product was isolated as a pale yellow solid after purification by silica gel flash chromatography with a 15 : 1 hexanes : ethyl acetate eluent. Yield: 52%. ^{1}H NMR (400 MHz, 298 K, CD_2Cl_2) δ_H (ppm): 7.69–7.64 (m, 8H), 7.61–7.59 (m, 2H), 7.39–7.36 (m, 2H), 7.31–7.29 (m, 12H). $^{13}C\{^1H\}$ NMR (101 MHz, 298 K, CD_2Cl_2) δ_C (ppm): 136.6 (d, $J = 6.7$ Hz), 133.1 (d, $J = 1.8$ Hz), 133.0 (d, $J = 21.1$ Hz), 129.4 (d, $J = 38.0$ Hz), 129.3, 129.3, 125.7, 106.6 (d, $J = 3.7$ Hz), 91.0 (d, $J = 9.2$ Hz). $^{31}P\{^1H\}$ NMR (161 MHz, 298 K, CD_2Cl_2) δ_P (ppm): −33.11 (s). HRMS-ESI: *m*/*z* 495.1426 $(M + H)^+$. IR (KBr) $\tilde{\nu}$ (cm^{-1}): 630, 808, 873 (P–C≡C), 2161 (C≡C). DSC: 78 °C (melt), 266 °C (maximum). Elemental analysis, calcd for $C_{34}H_{24}P_2$: C, 82.58; H, 4.89. Found: C, 82.18; H, 4.74.

*1,2-Bis((bis(4-methoxyphenyl)phosphino)ethynyl)benzene, dppeb-pOCH$_3$ (**1b**).* To a solution of EDTMS (1.30 g, 4.80 mmol) in 125 mL THF at 0 °C was added 1.6 M *n*-BuLi in hexanes (6.29 mL, 10.07 mmol), resulting in an immediate color change from pale yellow to dark brown. The mixture was slowly warmed to 55 °C leading to a gradual color change to light, milky brown. After stirring for 2 h at elevated temperature the mixture was again cooled to 0 °C and a solution of chlorobis(4-methoxyphenyl)phosphine (2.69 g, 10.55 mmol) in 25 mL THF was added. The solution gradually became dark brown and cleared upon phosphine addition. The mixture was warmed to RT and stirred for 3 h. The product was isolated as an off-white solid after purification using silica gel flash chromatography with a 100% benzene eluent. Yield: 63%. ^{1}H NMR (400 MHz, 298 K, CD_2Cl_2) δ_H (ppm): 7.60–7.55 (m, 10H), 7.36–7.34 (m, 2H), 6.85–6.81 (m, 8H), 3.76 (s, 12H). $^{13}C\{^1H\}$ NMR (101 MHz, 298 K, CD_2Cl_2) δ_C (ppm): 160.1, 133.7, 133.5, 132.0 (d, $J = 3.1$ Hz), 126.8 (d, $J = 6.3$ Hz), 124.8, 113.9 (d, $J = 13.9$ Hz), 105.0 (d, $J = 5.2$ Hz), 91.1 (d, $J = 15.2$ Hz), 54.7. $^{31}P\{^1H\}$ NMR (161 MHz, 298 K, CD_2Cl_2) δ_P (ppm): −36.72. HRMS-ESI MS: *m*/*z* 615.1850 $(M + H)^+$. IR (KBr) $\tilde{\nu}$ (cm^{-1}): 624, 809, 871 (P–C≡C), 2161 (C≡C). DSC: 96 °C (melt), 264 °C (maximum). Elemental analysis, calcd for $C_{38}H_{32}O_4P_2$: C, 74.26; H, 5.25. Found: C, 73.97; H, 5.34.

*1,2-Bis((bis(4-(trifluoromethyl)phenyl)phosphino)ethynyl) benzene, dppeb-pCF$_3$ (**1c**).* To a solution of EDTMS (1.88 g, 6.93 mmol) in 125 mL THF at 0 °C was added 1.6 M *n*-BuLi in hexanes (9.09 mL, 14.56 mmol), resulting in an immediate color change from pale yellow to dark brown. The mixture was slowly warmed to 55 °C leading to a gradual color change to light, milky brown. After stirring for 2 h at elevated temperature the mixture was again cooled to 0 °C and a solution of chlorobis(4-(trifluoromethyl)phenyl)phosphine (5.00 g, 14.02 mmol) in 10 mL THF was added. The solution became clear, dark brown immediately upon phosphine addition. The mixture was warmed to RT and stirred for 3 h. The product was isolated as a yellow oil after purification using silica gel flash chromatography with a 10 : 1 hexanes:ethyl acetate eluent followed by a second purification using a 2 : 1 hexanes : dichloromethane eluent. Yield: 20%. ^{1}H NMR (400 MHz, 298 K, CD_2Cl_2) δ_H (ppm): 7.78–7.74 (m, 8H), 7.66–7.63 (m, 2H), 7.54–7.51 (m, 8H), 7.46–7.43 (m, 2H). $^{31}P\{^1H\}$ NMR (161 MHz, 298 K, CD_2Cl_2) δ_P (ppm): −32.75. ^{19}F NMR (400 MHz, 298 K, CD_2Cl_2) δ_F (ppm): −63.33. HRMS-ESI MS: *m*/*z* 767.0926 $(M + H)^+$. IR (KBr) $\tilde{\nu}$ (cm^{-1}): 628, 813, 873 (P–C≡C), 2163 (C≡C).

*1,2-Bis((bis(3,5-dimethylphenyl)phosphino)ethynyl)benzene, dppeb-m$_2$CH$_3$ (**1d**).* To a solution of EDTMS (2.09 g, 7.74 mmol) in 150 mL THF at to 0 °C was carefully added 1.6 M *n*-BuLi in hexanes (10.16 mL, 16.26 mmol) resulting in an immediate color change from pale yellow to dark brown. The reaction mixture was stirred for 2 h after slowly warming to 55 °C during which time the solution turned light brown and became milky. After 2 h, the reaction was cooled again to 0 °C and a solution of

chlorobis(3,5-dimethylphenyl)phosphine (5.00 g, 18.07 mmol) in 20 mL THF was added. After slowly warming to RT, the mixture was stirred for 3 h during which time the color darkened leaving a clear brown solution. The product was obtained as a white solid after purification by silica gel flash chromatography using a 20 : 1 hexanes : ethyl acetate eluent. Crystals suitable for characterization by X-ray crystallography were grown from vapor diffusion of heptane into a saturated solution of dichloromethane at −20 °C. Yield: 63%. ^{1}H NMR (400 MHz, 298 K, CD_2Cl_2) δ_H (ppm): 7.60–7.57 (m, 2H), 7.37–7.35 (m, 2H), 7.23 (d, J = 11.2 Hz, 8H), 6.93 (br s, 4H), 2.24 (s, 24 H). ^{13}C{^{1}H} NMR (101 MHz, 298 K, CD_2Cl_2) δ_C (ppm): 138.7 (d, J = 8.2 Hz), 136.2 (d, J = 6.5 Hz), 132.8, 131.3, 130.8, 130.6, 129.1, 125.9, 106.4 (d, J = 3.8 Hz), 91.7 (d, J = 10.0 Hz), 21.6. ^{31}P{^{1}H} NMR (161 MHz, 298 K, CD_2Cl_2) δ_P (ppm): −33.59. HRMS-ESI MS: m/z 607.2682 $(M + H)^+$. IR (KBr) $\tilde{\nu}$ (cm^{-1}): 630, 808, 873 (P–C≡C), 2161 (C≡C). DSC: 121 °C (melt), 271 °C (maximum). Elemental analysis, calcd for $C_{42}H_{40}P_2$: C, 83.14; H, 6.64. Found: C, 82.97; H, 6.55.

*1,2-Bis((bis(3,5-bis(trifluoromethyl)phenyl)phosphino)ethynyl) benzene, dppeb-m_2CF_3 (**1e**).* To a solution of EDTMS (1.88 g, 6.93 mmol) in 100 mL THF at 0 °C was added 1.6 M *n*-BuLi in hexanes (9.09 mL, 14.55 mmol) resulting in an immediate color change from yellow to dark brown. The solution was allowed to warm to 55 °C and was stirred at elevated temperature for 2 h during time which time the reaction mixture turned light brown and became milky. The solution was then cooled to 0 °C and bis(3,5-bis(trifluoromethyl)phenyl)chlorophosphine (7.51 g, 15.25 mmol) in 20 mL THF was added. The reaction mixture turned dark blue and was allowed to stir at RT for 3 h. The crude reaction mixture was filtered through a silica gel plug and washed with copious amounts of benzene and dichloromethane to remove impurities yielding a yellow/brown solution. The product was then isolated as an off-white solid after purification by silica gel flash chromatography with a 5 : 1 hexanes : ethyl acetate eluent. Crystals suitable for characterization by X-ray crystallography were grown from vapor diffusion of hexane into a saturated dichloromethane solution at −20 °C. Yield: 52%. ^{1}H NMR (400 MHz, 298 K, CD_2Cl_2) δ_H (ppm): 8.07 (d, J = 7.6 Hz, 8H), 7.89 (s, 4H), 7.68–7.66 (m, 2H), 7.52–7.50 (m, 2H). ^{13}C{^{1}H} NMR (125 MHz, 298 K, CD_2Cl_2) δ_C (ppm): 138.8 (d, J = 13.7 Hz), 133.0 (d, J = 38.8 Hz), 133.0 (d, J = 22.1 Hz), 132.9 (q of d, J = 33.5 Hz, J = 7.3 Hz), 130.6, 124.9, 124.5 (m), 123.6 (q, J = 273.1 Hz), 109.5 (d, J = 6.2 Hz), 86.9 (d, J = 20.2 Hz). ^{31}P{^{1}H} NMR (161 MHz, 298 K, CD_2Cl_2) δ_P (ppm): −31.96. ^{19}F NMR (400 MHz, 298 K, CD_2Cl_2) δ_F (ppm): −63.28. HRMS-ESI MS: m/z 1073.0009 $(M + Cl)^-$. IR (KBr) $\tilde{\nu}$ (cm^{-1}): 634, 806, 877 (P–C≡C), 2167 (C≡C). DSC: 144 °C (melt), 275 °C (maximum). Elemental analysis, calcd for $C_{42}H_{16}F_{24}P_2$: C, 48.58; H, 1.55. Found: C, 48.40; H, 1.56.

*1,2-Bis((diisopropylphosphino)ethynyl)benzene, dipeb (**1f**).* To a solution of EDTMS (2.14 g, 7.92 mmol) in 125 mL of THF at 0 °C was added 1.6 M *n*-BuLi in hexanes (10.39 mL, 16.63 mmol) resulting in an immediate color change from pale yellow to dark brown. The mixture was slowly warmed to 55 °C and stirred for 2 h during which time the reaction color lightened to milky brown. After stirring at elevated temperature, the solution was cooled to 0 °C and a solution of chlorodiisopropylphosphine (2.77 mL, 17.42 mmol) in 10 mL THF was added. Upon slow warming to RT, the reaction mixture became a clear, dark brown solution which was stirred for 3 h. The product was isolated as a yellow oil after purification with silica gel flash chromatography using a 5 : 1 hexanes : benzene eluent. Yield: 81%. ^{1}H NMR (400 MHz, 298 K, CD_2Cl_2) δ_H (ppm): 7.47–7.44 (m, 2H), 7.27–7.25 (m, 2H), 2.02–1.95 (m, 4H), 1.26 (d, J = 11.2 Hz, 6H), 1.24 (d, J = 11.2 Hz, 6H), 1.16 (d, J = 16.8 Hz, 6H), 1.15 (d, J = 17.2 Hz, 6H). ^{13}C{^{1}H} NMR (101 MHz, 298 K, CD_2Cl_2) δ_C (ppm): 133.1, 128.5, 126.0, 104.1 (d, J = 4.7 Hz), 92.3 (d, J = 27.3 Hz), 24.5 (d, J = 8.8 Hz), 20.2 (d, J = 19.7 Hz), 19.9 (d, J = 6.8 Hz). ^{31}P{^{1}H} NMR (161 MHz, 298 K, CD_2Cl_2) δ_P (ppm): −11.79. HRMS-ESI MS: m/z 359.2042 $(M + H)^+$. IR (KBr) $\tilde{\nu}$ (cm^{-1}): 636, 802, 871 (P–C≡C), 2158 (C≡C).

*1,2-Bis((dicyclohexylphosphino)ethynyl)benzene, dcpeb (**1g**).* To a solution of EDTMS (2.33 g, 8.61 mmol) in 150 mL THF at 0 °C was added 1.6 M *n*-BuLi in hexanes (11.30 mL, 18.08 mmol) and the reaction mixture allowed to warm slowly to 55 °C. The reaction was stirred at elevated temperature for 2 h during which time the clear, dark brown solution lightened considerably and became milky. After 2 h, the solution was cooled to 0 °C and a solution of chlorodicyclohexylphosphine (4.18 mL, 18.94 mmol) in 10 mL THF was added. The mixture was slowly warmed to RT during which time the color darkened resulting in a clear brown solution after stirring for 3 h. The product was isolated as a yellow oil after purification by silica gel flash chromatography with a 10 : 1 hexanes : benzene eluent. Yield: 74%. ^{1}H NMR (400 MHz, 298 K, CD_2Cl_2) δ_H (ppm): 7.46–7.43 (m, 2H), 7.27–7.24 (m, 2H), 2.02–2.00 (m, 4H), 1.82–1.80 (m, 18H), 1.71–1.68 (m, 4H), 1.42–1.24 (m, 18H). ^{13}C{^{1}H} NMR (101 MHz, 298 K, CD_2Cl_2) δ_C (ppm): 133.1, 128.4, 126.2, 104.4 (d, J = 3.64 Hz), 92.6 (d, J = 26.4 Hz), 33.7 (d, J = 8.7 Hz), 30.8 (d, J = 18.0 Hz), 30.2 (d, J = 4.9 Hz), 27.7 (d, J = 18.7 Hz), 27.7 (d, J = 2.3 Hz), 27.0. ^{31}P{^{1}H} NMR (161 MHz, 298 K, CD_2Cl_2) δ_P (ppm): −20.80. HRMS-ESI MS: m/z 519.3329 $(M + H)^+$. IR (KBr) $\tilde{\nu}$ (cm^{-1}): 626, 800, 885 (P–C≡C), 2159 (C≡C).

*1,2-Bis((di-tert-butylphosphino)ethynyl)benzene, dtpeb (**1h**).* To a solution of EDTMS (2.02 g, 7.48 mmol) in 150 mL THF at 0 °C was added 1.6 M *n*-BuLi in hexanes (9.81 mL, 15.71 mmol). The solution immediately changed color from pale yellow to dark brown. The reaction mixture was heated to 50 °C and allowed to stir for 2 h during which time the solution color lightened, and the consistency became milky. The mixture was then cooled to 0 °C and a solution of di-*tert*-butylchlorophosphine (3.12 mL, 16.45 mmol) in 20 mL THF was added, resulting in an instantaneous color change to dark brown and a clearing of the cloudy solution. The mixture was slowly warmed to RT and stirred for 3 h. The product was isolated as a yellow oil after purification by silica gel flash chromatography using a 5 : 1 hexanes:benzene eluent. Yield: 64%. ^{1}H NMR (400 MHz, 298 K, CD_2Cl_2) δ_H (ppm): 7.49–7.47 (m, 2H), 7.28–7.26 (m, 2H), 1.29 (d, J = 12.4 Hz, 36H). ^{13}C{^{1}H} NMR (101 MHz, 298 K, CD_2Cl_2) δ_C (ppm): 133.3, 128.4, 126.0, 104.7 (d, J = 3.6 Hz), 93.8 (d, J = 25.3 Hz), 33.5 (d, J = 17.1 Hz), 30.2 (d, J = 14.6 Hz). ^{31}P{^{1}H} NMR (161 MHz, 298 K, CD_2Cl_2) δ_P (ppm): 12.33. HRMS-ESI MS: m/z 415.2700 $(M + H)^+$. IR (KBr) $\tilde{\nu}$ (cm^{-1}): 640, 802, 867 (P–C≡C), 2159 (C≡C).

Synthesis of phosphine oxide enediyne compounds (2b–2h)

General procedure for the synthesis of phosphine oxide enediynes. Syntheses for the phosphine oxide enediyne ligands were adapted from a published literature procedure[100] and performed under ambient conditions. To a solution of enediyne (**1b–1h**) (1 eq.) in 8 mL benzene was added excess hydrogen peroxide (30% by wt). The mixture was stirred vigorously at RT for 1 h after which time Na_2SO_4 was added. The reaction mixture was filtered and then evaporated to dryness to yield the final product (**2b–2h**). The phosphine oxide ligand 1,2-phenylenebis(ethyne-2,1-diyl)bis(diphenylphosphine oxide) (**2a**) has been reported previously.[41]

*1,2-Phenylenebis(ethyne-2,1-diyl)bis(bis(4-methoxyphenyl) phosphine) oxide (**2b**).* The product was isolated as a yellow oil. Yield: 81%. ^{1}H NMR (400 MHz, 298 K, CD_2Cl_2) δ_H (ppm): 7.77–7.72 (m, 8H), 7.69–7.67 (m, 2H), 7.50–7.47 (m, 2H), 6.94–6.91 (m, 8H), 3.81 (s, 12H). $^{13}C\{^1H\}$ NMR (101 MHz, 298 K, CD_2Cl_2) δ_C (ppm): 163.3, 134.1, 133.3 (d, J = 12.7 Hz), 130.9, 125.7, 124.4, 114.8 (d, J = 14.6 Hz), 101.7 (d, J = 28.5 Hz), 89.1 (d, J = 160.4 Hz), 55.9. $^{31}P\{^1H\}$ NMR (161 MHz, 298 K, CD_2Cl_2) δ_P (ppm): 7.56. HRMS-ESI MS: m/z 647.1756 $(M + H)^+$. IR (KBr) $\tilde{\nu}$ (cm^{-1}): 626, 819, 875 (P–C≡C), 1203 (P═O), 2177 (C≡C). Elemental analysis, calcd for $C_{38}H_{32}P_2O_6 \cdot H_2O$: C, 68.67; H, 5.15. Found: C, 68.73; H, 5.19.

*1,2-Phenylenebis(ethyne-2,1-diyl)bis(bis(4-(trifluoromethyl) phenyl)-phosphine) oxide (**2c**).* The product was isolated as a yellow oil. Yield: 67%. ^{1}H NMR (400 MHz, 298 K, CD_2Cl_2) δ_H (ppm): 8.06–8.01 (m, 8H), 7.76–7.71 (m, 10H), 7.59–7.57 (m, 2H). $^{13}C\{^1H\}$ NMR (101 MHz, 298 K, CD_2Cl_2) δ_C (ppm): 137.0 (d, J = 121.2 Hz), 134.6 (dd, J = 33.1 Hz, J = 3.3 Hz), 134.3 (d, J = 1.9 Hz), 132.0 (d, J = 11.7 Hz), 131.8, 126.5 (q, J = 3.6 Hz), 126.4 (q, J = 4.0 Hz), 125.4, 123.4, 122.7, 103.7 (d, J = 30.0 Hz), 86.9 (d, J = 169.4). $^{31}P\{^1H\}$ NMR (161 MHz, 298 K, CD_2Cl_2) δ_P (ppm): 4.16. ^{19}F NMR (400 MHz, 298 K, CD_2Cl_2) δ_F (ppm): −64.56. HRMS-ESI MS: m/z 799.0818 $(M + H)^+$. IR (KBr) $\tilde{\nu}$ (cm^{-1}): 630, 823, 879 (P–C≡C), 1215 (P═O), 2179 (C≡C).

*1,2-Phenylenebis(ethyne-2,1-diyl)bis(bis(3,5-dimethylphenyl) phosphine) oxide (**2d**).* The product was isolated as a shiny white solid. Crystals suitable for characterization by X-ray crystallography were grown from vapor diffusion of pentane into a saturated dichloromethane solution at −20 °C. Yield: 93%. ^{1}H NMR (400 MHz, 298 K, CD_2Cl_2) δ_H (ppm): 7.71–7.69 (m, 2H), 7.51–7.49 (m, 2H), 7.45 (d, J = 16.0 Hz, 8H), 7.09 (br s, 4H), 2.26 (s, 24H). $^{13}C\{^1H\}$ NMR (101 MHz, 298 K, CD_2Cl_2) δ_C (ppm): 139.1 (d, J = 14.2 Hz), 134.4 (d, J = 3.1 Hz), 134.2, 134.1, 132.9, 130.9, 128.8 (d, J = 11.1 Hz), 123.9, 101.8 (d, J = 27.8 Hz), 89.0 (d, J = 158.9 Hz), 21.5. $^{31}P\{^1H\}$ NMR (161 MHz, 298 K, CD_2Cl_2) δ_P (ppm): 8.42. HRMS-ESI MS: m/z 639.2575 $(M + H)^+$. IR (KBr) $\tilde{\nu}$ (cm^{-1}): 640, 809, 875 (P–C≡C), 1199 (P═O), 2177 (C≡C). DSC: 153 °C (melt), no maximum up to 280 °C. Elemental analysis, calcd for $C_{42}H_{40}P_2O_2 \cdot C_6H_6 \cdot H_2O$: C, 78.46; H, 6.59. Found: C, 78.13; H, 6.28.

*1,2-Phenylenebis(ethyne-2,1-diyl)bis(bis(3,5-bis(trifluoromethyl) phenyl)-phosphine) oxide (**2e**).* Due to the low solubility of **1e** in benzene, a 1 : 1 solvent mixture of benzene : dichloromethane was utilized. The product was isolated as an off-white solid. Crystals suitable for characterization by X-ray crystallography were grown from vapor diffusion of pentane into a saturated dichloromethane solution at −20 °C. Yield: 88%. ^{1}H NMR (400 MHz, 298 K, CD_2Cl_2) δ_H (ppm): 8.37 (d, J = 15.6 Hz, 8H), 8.10 (s, 4H), 7.82–7.80 (m, 2H), 7.66–7.64 (m, 2H). $^{13}C\{^1H\}$ NMR (101 MHz, 298 K, CD_2Cl_2) δ_C (ppm): 135.4 (d, J = 123.4 Hz), 134.0, 133.0 (q of d, J = 34.2 Hz, J = 13.9 Hz), 132.3, 131.8 (d, J = 12.9 Hz), 127.4, 124.7, 122.0, 105.3 (d, J = 31.9 Hz), 85.7 (d, J = 176.4 Hz). $^{31}P\{^1H\}$ NMR (161 MHz, 298 K, CD_2Cl_2) δ_P (ppm): 1.83. ^{19}F NMR (400 MHz, 298 K, CD_2Cl_2) δ_F (ppm): −64.26. HRMS-ESI MS: m/z 1071.0302 $(M + H)^+$. IR (KBr) $\tilde{\nu}$ (cm^{-1}): 646, 809, 885 (P–C≡C), 1216 (P═O), 2181 (C≡C). DSC: 164 °C (melt), no maximum up to 280 °C. Elemental analysis, calcd for $C_{42}H_{16}F_{24}P_2O_2$: C, 47.12; H, 1.51. Found: C, 46.87; H, 1.49.

*1,2-Phenylenebis(ethyne-2,1-diyl)bis(diisopropylphosphine oxide) (**2f**).* The product was isolated as a yellow oil. Yield: 66%. ^{1}H NMR (400 MHz, 298 K, CD_2Cl_2) δ_H (ppm): 7.62–7.60 (m, 2H), 7.46–7.44 (m, 2H), 2.19–2.10 (m, 4H), 1.30 (d, J = 7.2 Hz, 6H), 1.28 (d, J = 6.8 Hz, 6H), 1.25 (d, J = 7.2 Hz, 6H), 1.24 (d, J = 6.8 Hz, 6H). $^{13}C\{^1H\}$ NMR (101 MHz, 298 K, CD_2Cl_2) δ_C (ppm): 134.0, 130.6, 124.0, 100.2 (d, J = 20.3 Hz), 86.4 (d, J = 129.4 Hz), 28.1, 27.3, 16.6 (d, J = 2.7 Hz), 15.3 (d, J = 3.2 Hz). $^{31}P\{^1H\}$ NMR (161 MHz, 298 K, CD_2Cl_2) δ_P (ppm): 42.65. HRMS-ESI MS: m/z 391.1954 $(M + H)^+$. IR (KBr) $\tilde{\nu}$ (cm^{-1}): 667, 813, 873 (P–C≡C), 1180 (P═O), 2177 (C≡C).

*1,2-Phenylenebis(ethyne-2,1-diyl)bis(dicyclohexylphosphine oxide) (**2g**).* The product was isolated as a yellow oil. Yield: 94%. ^{1}H NMR (400 MHz, 298 K, CD_2Cl_2) δ_H (ppm): 7.63–7.60 (m, 2H), 7.46–7.43 (m, 2H), 2.04–1.83 (m, 20H), 1.74–1.71 (m, 4H), 1.56–1.46 (m, 8H), 1.36–1.23 (m, 12H). $^{13}C\{^1H\}$ NMR (101 MHz, 298 K, CD_2Cl_2) δ_C (ppm): 133.9 (d, J = 1.8 Hz), 130.5, 124.1 (m), 100.0 (d, J = 20.0 Hz), 87.3 (d, J = 128.4 Hz), 37.3 (d, J = 78.5 Hz), 26.8 (d, J = 7.2 Hz), 26.7 (d, J = 6.7 Hz), 26.5 (d, J = 3.2 Hz), 26.4 (d, J = 5.0 Hz), 25.3 (d, J = 3.3 Hz). $^{31}P\{^1H\}$ NMR (161 MHz, 298 K, CD_2Cl_2) δ_P (ppm): 35.80. HRMS-ESI MS: m/z 551.3213 $(M + H)^+$. IR (KBr) $\tilde{\nu}$ (cm^{-1}): 632, 808, 873 (P–C≡C), 1211 (P═O), 2177 (C≡C).

*1,2-Phenylenebis(ethyne-2,1-diyl)bis(di-tert-butylphosphine oxide) (**2h**).* The product was isolated as a yellow oil. Yield: 75%. ^{1}H NMR (400 MHz, 298 K, CD_2Cl_2) δ_H (ppm): 7.63–7.61 (m, 2H), 7.47–7.45 (m, 2H), 1.37 (d, J = 15.2 Hz, 36H). $^{13}C\{^1H\}$ NMR (101 MHz, 298 K, CD_2Cl_2) δ_C (ppm): 134.2, 130.5, 124.0, 100.4 (d, J = 17.2 Hz), 87.3 (d, J = 121.1 Hz), 37.1, 36.3, 26.8. $^{31}P\{^1H\}$ NMR (161 MHz, 298 K, CD_2Cl_2) δ_P (ppm): 49.41. HRMS-ESI MS: m/z 447.2585 $(M + H)^+$. IR (KBr) $\tilde{\nu}$ (cm^{-1}): 644, 815, 869 (P–C≡C), 1220 (P═O), 2175 (C≡C). Elemental analysis, calcd for $C_{26}H_{40}P_2O_2 \cdot H_2O_2$: C, 64.98; H, 8.81. Found: C, 64.77; H, 8.63.

Synthesis of Pt(II) phosphine enediyne dichloride complexes (3a–3g)

*Dichloro-(1,2-bis((diphenylphosphino)ethynyl)benzene)platinum(II), Pt(dppeb)Cl$_2$ (**3a**).* This complex has been generated *in situ* previously.[35,43] Using the procedure detailed here, the complex has now been isolated and characterized. To a solution of Pt(cod)Cl_2 (64.1 mg, 0.171 mmol) in 6 mL DCM was added a solution of **1a** (102 mg, 0.206 mmol) in 6 mL DCM. The mixture was allowed to stir at RT for 30 min, then the solvent was removed *in vacuo*. The residue was suspended in minimal DCM and filtered to remove insoluble material. To the filtrate was added excess hexanes. The resulting off-white precipitate

was collected, washed with hexanes, and dried. Crude yield: 53%. The crude precipitate was purified by preparatory chromatography on silica gel with a 50 : 1 DCM : acetone eluent (R_f = 0.57). Purified yield: 31%. ^{1}H NMR (400 MHz, 298 K, CD_2Cl_2) δ_H (ppm): 7.93–7.87 (m, 8H), 7.53–7.42 (m, 16H). $^{31}P\{^1H\}$ NMR (161 MHz, 298 K, CD_2Cl_2) δ_P (ppm): −17.44 (s, J_{P-Pt} = 3823 Hz). HRMS-ESI MS: *m*/*z* 725.0702 (M–Cl)$^+$. IR (KBr) $\tilde{\nu}$ (cm^{-1}): 637, 820, 882 (P–C≡C), 2171 (C≡C). DSC: 116 °C (maximum).

*Dichloro-(1,2-bis((bis(4-methoxyphenyl)phosphino)ethynyl) benzene) platinum(II), Pt(dppeb-pOCH$_3$)Cl$_2$ (**3b**).* To a solution of Pt(cod)Cl$_2$ (57.2 mg, 0.153 mmol) in 10 mL DCM at 0 °C was added a solution of **1b** (113 mg, 0.184 mmol) in 5 mL DCM, also at 0 °C. The mixture was allowed to stir on ice for 30 min after which time the solvent was removed by rotary evaporation at 0 °C. The resulting residue was dissolved in minimal DCM and excess hexanes added. The off-white precipitate was isolated by filtration, washed with hexanes, and dried. Crude yield: 43%. The crude precipitate was purified by preparatory chromatography on silica gel with a 20 : 1 DCM : acetone eluent (R_f = 0.65). Purified yield: 20% ^{1}H NMR (400 MHz, 298 K, CD_2Cl_2) δ_H (ppm): 7.83–7.78 (m, 8H), 7.52–7.46 (m, 4H), 6.96–6.93 (m, 8H), 3.85 (s, 12H). $^{31}P\{^1H\}$ NMR (161 MHz, 298 K, CD_2Cl_2) δ_P (ppm): −19.13 (s, J_{P-Pt} = 3846 Hz). HRMS-ESI MS: *m*/*z* 844.1100 (M–Cl)$^+$. IR (KBr) $\tilde{\nu}$ (cm^{-1}): 620, 823, 881 (P–C≡C), 2167 (C≡C). DSC: 120 °C (maximum).

*Dichloro-(1,2-bis((bis(4-(trifluoromethyl)phenyl)phosphino) ethynyl)benzene) platinum(II), Pt(dppeb-pCF$_3$)Cl$_2$ (**3c**).* To a solution of Pt(cod)Cl$_2$ (25.7 mg, 0.069 mmol) in 15 mL DCM was added a solution of **1c** (63.2 mg, 0.083 mmol) in 10 mL DCM. The mixture was stirred at RT for 30 min and then the solvent was removed *in vacuo*. The residue was dissolved in minimal DCM, followed by the addition of excess hexanes. The off-white precipitate was filtered, washed with hexanes, and dried. Crude yield: 45%. The crude solid was stirred in cold Et$_2$O for 2 min and then filtered resulting in an off-white solid. Purified yield: 17% ^{1}H NMR (400 MHz, 298 K, CD_2Cl_2) δ_H (ppm): 8.05–8.00 (m, 8H), 7.73–7.71 (m, 8H), 7.58 (s, 4H). $^{31}P\{^1H\}$ NMR (161 MHz, 298 K, CD_2Cl_2) δ_P (ppm): −17.65 (s, J_{P-Pt} = 3797 Hz). ^{19}F NMR (400 MHz, 298 K, CD_2Cl_2) δ_F (ppm): −63.59. HRMS-ESI MS: *m*/*z* 996.0226 (M–Cl)$^+$. IR (KBr) $\tilde{\nu}$ (cm^{-1}): 630, 829, 883 (P–C≡C), 2175 (C≡C). DSC: 177 °C (maximum).

*Dichloro-(1,2-bis((bis(3,5-dimethylphenyl)phosphino)ethynyl) benzene) platinum(II), Pt(dppeb-m$_2$CH$_3$)Cl$_2$ (**3d**).* To a solution of Pt(cod)Cl$_2$ (82.1 mg, 0.219 mmol) in 10 mL DCM was added a solution of **1d** (111 mg, 0.183 mmol) in 5 mL DCM. The mixture was stirred at RT for 30 min and then solvent was removed under reduced pressure. The remaining residue was dissolved in minimal DCM and excess hexanes added to induce precipitation. An off-white solid was filtered, washed with hexanes, and dried. Crude yield: 92%. The product was purified by preparatory chromatography on silica gel with a 2 : 1 hexanes : acetone eluent (R_f = 0.63). Purified yield: 56%. ^{1}H NMR (400 MHz, 298 K, CD_2Cl_2) δ_H (ppm): 7.54–7.52 (m, 2H), 7.49–7.43 (m, 10H), 7.11 (br s, 4H), 2.31 (s, 24H). $^{31}P\{^1H\}$ NMR (161 MHz, 298 K, CD_2Cl_2) δ_P (ppm): −16.53 (s, J_{P-Pt} = 3818 Hz). HRMS-ESI MS: *m*/*z* 837.1972 (M–Cl)$^+$. IR (KBr) $\tilde{\nu}$ (cm^{-1}): 635, 814, 883 (P–C≡C), 2163 (C≡C). DSC: 106 °C (maximum).

*Dichloro-(1,2-bis((bis(3,5-bis(trifluoromethyl)phenyl)phosphino) ethynyl)-benzene)platinum(II), Pt(dppeb-m$_2$CF$_3$)Cl$_2$ (**3e**).* To a solution of Pt(cod)Cl$_2$ (61.2 mg, 0.164 mmol) in 10 mL DCM was added a solution of **1e** (204 mg, 0.196 mmol) in 10 mL DCM. The mixture was stirred at RT for 30 min followed by solvent removal by rotary evaporation. The residue was dissolved in minimal DCM and filtered. To the filtrate was added excess hexanes to induce precipitation. The off-white precipitate was filtered, washed with hexanes and cold Et$_2$O, and dried. Crystals suitable for characterization by X-ray crystallography were grown from vapor diffusion of hexane into a saturated dichloromethane solution at −20 °C. Yield: 43%. ^{1}H NMR (400 MHz, 298 K, CD_2Cl_2) δ_H (ppm): 8.38 (d, J = 11.6 Hz, 8 H), 8.14 (s, 4H), 7.63 (s, 4H). $^{13}C\{^1H\}$ NMR (101 MHz, 298 K, CD_2Cl_2) δ_C (ppm): 134.3, 132.9 (q of d, J = 34.4 Hz, J = 12.8 Hz), 132.6, 131.7 (d, J = 80.9 Hz), 131.6, 127.0, 124.1, 123.2 (q, J = 273.3 Hz), 115.3 (d, J = 16.2 Hz), 84.1 (d, J = 112.9 Hz). $^{31}P\{^1H\}$ NMR (161 MHz, 298 K, CD_2Cl_2) δ_P (ppm): −18.17 (s, J_{P-Pt} = 3812 Hz). ^{19}F NMR (400 MHz, 298 K, CD_2Cl_2) δ_F (ppm): −64.23. HRMS-ESI MS: *m*/*z* 1268.9723 (M–Cl)$^+$. IR (KBr) $\tilde{\nu}$ (cm^{-1}): 655, 817, 885 (P–C≡C), 2175 (C≡C). DSC: 236 °C (maximum). Elemental analysis, calcd for $C_{42}H_{16}F_{24}P_2PtCl_2$: C, 38.67; H, 1.24. Found: C, 38.99; H, 1.07.

*Dichloro-(1,2-bis((diisopropylphosphino)ethynyl)benzene)platinum(II), Pt(dipeb)Cl$_2$ (**3f**).* To a solution of Pt(cod)Cl$_2$ (280 mg, 0.748 mmol) in 12 mL DCM was added a solution of **1f** (320 mg, 0.893 mmol) in 5 mL DCM. The mixture was allowed to stir at RT for 75 min after which time the solvent was removed by rotary evaporation. The resulting residue was dissolved in minimal DCM and excess hexanes added. The off-white precipitate was isolated by filtration, washed with hexanes, and dried. Crude yield: 80%. The crude precipitate was purified by preparatory chromatography on silica gel with a 10 : 1 benzene : acetone eluent (R_f = 0.58). Crystals suitable for characterization by X-ray crystallography were grown from vapor diffusion of pentane into a saturated dichloromethane solution at −20 °C. Purified yield: 49%. ^{1}H NMR (400 MHz, 298 K, CD_2Cl_2) δ_H (ppm): 7.59–7.57 (m, 2H), 7.53–7.51 (m, 2H), 3.01–2.97 (m, 4H), 1.45 (d, J = 7.0 Hz, 6H), 1.41 (d, J = 7.0 Hz, 6H), 1.37 (d, J = 7.0 Hz, 6H), 1.34 (d, J = 7.0 Hz, 6H). $^{13}C\{^1H\}$ NMR (101 MHz, 298 K, CD_2Cl_2) δ_C (ppm): 130.1, 129.7, 125.1, 110.1, 85.3 (d, J = 5.7 Hz), 84.7 (d, J = 5.5 Hz), 27.9 (d, J = 42.4 Hz), 20.3, 19.0. $^{31}P\{^1H\}$ NMR (161 MHz, 298 K, CD_2Cl_2) δ_P (ppm): 13.46 (s, J_{P-Pt} = 3815 Hz). HRMS-ESI MS: *m*/*z* 589.1321 (M–Cl)$^+$. IR (KBr) $\tilde{\nu}$ (cm^{-1}): 634, 827, 881 (P–C≡C), 2163 (C≡C). DSC: 139 °C (maximum). Elemental analysis, calcd for $C_{22}H_{32}P_2PtCl_2$: C, 42.32; H, 5.17. Found: C, 42.04; H, 4.89.

*Dichloro-(1,2-bis((dicyclohexylphosphino)ethynyl)benzene)platinum(II), Pt(dcpeb)Cl$_2$ (**3g**).* To a solution of Pt(cod)Cl$_2$ (115 mg, 0.307 mmol) in 10 mL DCM was added a solution of **1g** (191 mg, 0.369 mmol) in 5 mL DCM. The mixture was allowed to stir at RT for 2 h after which time the solvent was removed by rotary evaporation. The resulting residue was dissolved in minimal DCM and excess hexanes added. The off-white precipitate was then filtered, washed with hexanes, and dried. Crude yield: 72% The crude precipitate was purified by preparatory

chromatography on silica gel with a 10 : 1 benzene : acetone eluent ($R_f = 0.75$). Purified yield: 46%. ^{1}H NMR (400 MHz, 298 K, CD_2Cl_2) δ_H (ppm): 7.59–7.57 (m, 2H), 7.52–7.50 (m, 2H), 2.77–2.69 (m, 4H), 2.39 (br s, 4H), 1.99–1.96 (m, 4H), 1.81 (br s, 8H), 1.70–1.65 (m, 8H), 1.57–1.51 (m, 6H), 1.40–1.21 (m, 10H). ^{31}P{^{1}H} NMR (161 MHz, 298 K, CD_2Cl_2) δ_P (ppm): 4.35 (s, J_{P-Pt} = 3822 Hz). HRMS-ESI MS: m/z 749.2589 (M–Cl)$^+$. IR (KBr) $\tilde{\nu}$ (cm^{-1}): 642, 827, 889 (P–C≡C), 2163 (C≡C). DSC: 140 °C (maximum).

Bergman cyclization of Pt(II) phosphine enediyne dichloride complexes and isolation of cyclized products (4a–4f)

General procedure for the Bergman cyclization of Pt(II) phosphine enediyne complexes and the determination of cycloaromatization rate. Pt(II) phosphine enediyne dichloride complexes were purified as described above directly before use. Metalloenediynes (**3a–3g**) were dissolved in $CDCl_3$, dried over 4 Å molecular sieves, to give solutions of 3–30 mM, depending on solubility. A slight molar excess of triphenylphosphine oxide, Ph_3PO, was then added as an internal ^{31}P NMR standard followed by 100 equivalents of 1,4-cyclohexadiene. The solution was sealed in an NMR tube under ambient conditions and maintained in a temperature-controlled bath or in the NMR spectrometer. ^{31}P NMR spectra were acquired at $t = 0$, 2, 4, 8, 12, 24, 36 h… or $t = 0$, 1, 2, 3, 4 h… time intervals for complexes with cyclization $t_{1/2}$ > 12 h and $t_{1/2}$ < 12 h, respectively. The disappearance of the starting material was followed to at least 90% completion by integration of the Pt(II) phosphine enediyne dichloride ^{31}P NMR signal (**3a–3g**) *vs.* that of Ph_3PO. Cyclization was monitored in 5 °C increments for each complex: **3b** (5–20 °C); **3a**, **3d** (10–25 °C); **3c** (15, 25–35 °C); **3e–3g** (25–40 °C), and data were collected in triplicate. Complex **3c** contained ∼5% Pt(cod)Cl_2 impurity. Rate constants were obtained from highly linear first order kinetic plots (R^2 > 0.98) and the free energy of activation ($\Delta G^{\ddagger}$) was calculated from standard Eyring plots. The cyclization of all complexes except of **3g** proceeds cleanly to the corresponding cyclized product in >90% yield. Due to the low concentrations used during the kinetic experiments (3–30 mM), the reaction mixtures from all trials for a given compound were combined prior to purification with preparatory silica gel chromatography. Following purification, all cyclized compounds were fully characterized.

*Dichloro-(2,3-bis(diphenylphosphino)naphthalene)platinum(II), Pt(dppnap)Cl_2 (**4a**).* This complex has been reported previously using a different synthetic protocol.[43] After completion of the kinetic experiments described above (3.9–7.4 mM solutions), the product was isolated as a white solid using silica gel preparatory chromatography with a 50 : 1 DCM : acetone eluent ($R_f = 0.45$). Crystals suitable for characterization by X-ray crystallography were grown from slow evaporation of a saturated solution in CD_2Cl_2 at room temperature. ^{1}H NMR (400 MHz, 298 K, CD_2Cl_2) δ_H (ppm): 8.12–8.09 (m, 2H), 7.89–7.87 (m, 2H), 7.81–7.75 (m, 8H), 7.67–7.64 (m, 2H), 7.55–7.51 (m, 4H), 7.47–7.43 (m, 8H). ^{13}C{^{1}H} NMR (101 MHz, 298 K, CD_2Cl_2) δ_C (ppm): 134.6, 134.5, 134.4, 132.4, 130.2, 129.4, 129.3, 129.2, 129.1. ^{31}P{^{1}H} NMR (161 MHz, 298 K, CD_2Cl_2) δ_P (ppm): 39.42 (s, J_{P-Pt} = 3597 Hz). HRMS-ESI MS: m/z 726.0851 (M–Cl)$^+$. Elemental analysis, calcd for $C_{34}H_{26}P_2PtCl_2$: C, 53.56; H, 3.44. Found: C, 53.75; H, 3.23.

*Dichloro-(2,3-bis(bis(4-methoxyphenyl)phosphino)naphthalene) platinum(II), Pt(dppnap-pOCH_3)Cl_2 (**4b**).* After completion of the kinetic experiments described above (3.4–8.9 mM solutions), the product was isolated as a white solid using silica gel preparatory chromatography with a 20 : 1 DCM : acetone eluent ($R_f = 0.56$). ^{1}H NMR (400 MHz, 298 K, CD_2Cl_2) δ_H (ppm): 8.08–8.05 (m, 2H), 7.90–7.87 (m, 2H), 7.71–7.66 (m, 10H), 6.98–6.95 (m, 8H), 3.84 (s, 12H). ^{13}C{^{1}H} NMR (101 MHz, 298 K, CD_2Cl_2) δ_C (ppm): 163.0, 136.2, 136.1, 136.0, 129.9, 129.2, 115.0, 114.9, 114.8, 56.0. ^{31}P{^{1}H} NMR (161 MHz, 298 K, CD_2Cl_2) δ_P (ppm): 37.19 (s, J_{P-Pt} = 3638 Hz). HRMS-ESI MS: m/z 847.1293 (M–Cl)$^+$.

*Dichloro-(2,3-bis(bis(4-(trifluoromethyl)phenyl)phosphino)naphthalene) platinum(II), Pt(dppnap-pCF_3)Cl_2 (**4c**).* After completion of the kinetic experiments described above (3.6–4.7 mM solutions), the product was isolated as an off-white solid using silica gel preparatory chromatography with a 2 : 1 hexanes:ethyl acetate eluent ($R_f = 0.57$). Crystals suitable for X-ray crystallographic analysis were grown from vapor diffusion of heptane into a saturated solution of dichloromethane. ^{1}H NMR (400 MHz, 298 K, CD_2Cl_2) δ_H (ppm): 8.17–8.14 (m, 2H), 7.97–7.90 (m, 10H), 7.77–7.74 (m, 10H). ^{13}C{^{1}H} NMR (101 MHz, 298 K, CD_2Cl_2) δ_C (ppm): 136.4 (d, J = 18.9 Hz), 135.3 (d, J = 6.8 Hz), 134.9 (d, J = 11.8 Hz), 134.5 (d, J = 33.0 Hz), 133.7 (d, J = 29.9 Hz), 132.5 (d, J = 67.0 Hz), 131.2, 129.4, 126.6–126.4 (m), 124.0 (q, J = 273.8 Hz). ^{31}P{^{1}H} NMR (161 MHz, 298 K, CD_2Cl_2) δ_P (ppm): 38.93 (s, J_{P-Pt} = 3553 Hz). ^{19}F NMR (400 MHz, 298 K, CD_2Cl_2) δ_F (ppm): −64.51. HRMS-ESI MS: m/z 998.0370 (M–Cl)$^+$.

*Dichloro-(2,3-bis(bis(3,5-dimethylphenyl)phosphino) naphthalene) platinum(II), Pt(dppnap-m$_2CH_3$)Cl_2 (**4d**).* After completion of the kinetic experiments described above (9.7–16.3 mM solutions), the product was isolated as an off-white solid using silica gel preparatory chromatography with a 2 : 1 hexanes : acetone eluent ($R_f = 0.56$). Crystals suitable for characterization by X-ray crystallography were grown from vapor diffusion of cyclohexane into a saturated dichloromethane solution at −20 °C. ^{1}H NMR (400 MHz, 298 K, CD_2Cl_2) δ_H (ppm): 8.04–8.01 (m, 2H), 7.89–7.87 (m, 2H), 7.65–7.63 (m, 2H), 7.35 (d, J = 12.0 Hz, 8H), 7.15 (br s, 4H), 2.28 (s, 24H). ^{13}C{^{1}H} NMR (101 MHz, 298 K, CD_2Cl_2) δ_C (ppm): 139.1 (d, J = 12.7 Hz), 139.1, 134.1, 132.0 (d, J = 11.8 Hz), 132.0, 129.8, 129.2, 128.9, 128.2, 21.7. ^{31}P{^{1}H} NMR (161 MHz, 298 K, CD_2Cl_2) δ_P (ppm): 39.58 (s, J_{P-Pt} = 3614 Hz). HRMS-ESI MS: m/z 838.2087 (M–Cl)$^+$.

*Dichloro-(2,3-bis(bis(3,5-(trifluoromethyl)phenyl)phosphino) naphthalene) platinum(II), Pt(dppnap-m$_2CF_3$)Cl_2 (**4e**).* After completion of the kinetic experiments described above (2.8–3.3 mM solutions), the product was isolated as a white solid using silica gel preparatory chromatography with a 2 : 1 hexanes:acetone eluent ($R_f = 0.49$). Crystals suitable for characterization by X-ray crystallography were grown directly from the cyclization reaction mixture. ^{1}H NMR (400 MHz, 298 K, CD_2Cl_2) δ_H (ppm): 8.25–8.17 (m, 14H), 8.04–8.01 (m, 2H), 7.87–7.85 (m, 2H). ^{13}C{^{1}H} NMR (101 MHz, 298 K, CD_2Cl_2) δ_C (ppm): 137.2 (d, J = 18.4 Hz), 135.5 (d, J = 6.9 Hz), 134.1, 134.0, 133.5 (q of d, J = 21.9 Hz, J = 12.8 Hz), 132.4, 130.6 (d, J = 68.2 Hz), 129.7, 127.6, 123.0 (q, J = 273.5 Hz). ^{31}P{^{1}H} NMR (161 MHz, 298 K, CD_2Cl_2)

δ_P (ppm): 39.87 (s, J_{P-Pt} = 3519 Hz). ^{19}F NMR (400 MHz, 298 K, CD_2Cl_2) δ_F (ppm): −64.35. HRMS-ESI MS: *m*/*z* 1327.9443 $(M + Na)^+$. Elemental analysis, calcd for $C_{42}H_{18}F_{24}P_2PtCl_2$: C, 38.61; H, 1.39. Found: C, 38.33; H, 1.13.

*Dichloro-(2,3-bis(diisopropylphosphino)naphthalene)platinum(II), Pt(dipnap)Cl$_2$ (**4f**).* After completion of the kinetic experiments described above (21.1–30.0 mM solutions), the product was isolated as a white solid using silica gel preparatory chromatography with a 25 : 5 : 1 benzene : acetone :hexanes eluent (R_f = 0.48). Crystals suitable for characterization by X-ray crystallography were grown from vapor diffusion of heptane into a saturated dichloromethane solution at −20 °C. ^1H NMR (400 MHz, 298 K, CD_2Cl_2) δ_H (ppm): 8.28 (d, *J* = 9.2 Hz, 2H), 8.05–8.03 (m, 2H), 7.76–7.74 (m, 2H), 3.14–3.04 (m, 4H), 1.43 (d, *J* = 6.8 Hz, 6H), 1.39 (d, *J* = 6.8 Hz, 6H), 1.25 (d, *J* = 7.2 Hz, 6H), 1.21 (d, *J* = 7.2 Hz, 6H). $^{13}C\{^1H\}$ NMR (101 MHz, 298 K, CD_2Cl_2) δ_C (ppm): 134.5 (dd, *J* = 53.5 Hz, *J* = 24.9 Hz), 134.1 (m), 132.7 (m), 129.3, 128.6, 27.5 (d, *J* = 36.3 Hz), 19.1, 18.5. $^{31}P\{^1H\}$ NMR (161 MHz, 298 K, CD_2Cl_2) δ_P (ppm): 60.73 (s, J_{P-Pt} = 3576 Hz). HRMS-ESI MS: *m*/*z* 590.1482 $(M–Cl)^+$.

Synthesis of a dimeric Pt(II) phosphine enediyne complex

*Dichloro-(1,2-bis((bis(3,5-dimethylphenyl)phosphino)ethynyl) benzene) platinum(II) dimer, Pt$_2$(μ_2-dppeb-m$_2$CH$_3$)$_2$Cl$_4$ (**5d**).* To a solution of $Pt(cod)Cl_2$ (51.6 mg, 0.138 mmol) in 7 mL DCM was added a solution of **1d** (101 mg, 0.166 mmol) in 5 mL DCM. The mixture was allowed to stir at RT for 30 min after which time the solvent was removed *in vacuo*. The resulting residue was dissolved in minimal DCM and excess hexanes added. The off-white precipitate was filtered, washed with hexanes, and dried. Crystals suitable for characterization by X-ray crystallography were grown from vapor diffusion of hexane into a saturated dichloromethane solution at −20 °C. Yield: 61%. ^1H NMR (400 MHz, 298 K, CD_2Cl_2) δ_H (ppm): 7.69 (d, *J* = 13.6 Hz, 8H), 7.28–7.26 (m, 4H), 7.06 (br s, 4H), 6.99–6.95 (m, 12H), 6.26 (s, 4H), 2.31 (s, 24H), 1.84 (s, 24H). $^{13}C\{^1H\}$ NMR (101 MHz, 298 K, CD_2Cl_2) δ_C (ppm): 139.1–139.0 (m), 138.1–138.0 (m), 133.8, 133.2, 133.1 (t, *J* = 6.6 Hz), 133.0, 131.8 (d, *J* = 77.1 Hz), 130.4 (d, *J* = 5.4 Hz), 129.4, 123.4 (d, *J* = 75.1 Hz), 121.3, 110.4 (d, *J* = 19.8 Hz), 88.0 (dd, *J* = 112.8 Hz, 6.8 Hz), 21.7, 21.1. $^{31}P\{^1H\}$ NMR (161 MHz, 298 K, CD_2Cl_2) δ_P (ppm): −2.61 (s, J_{P-Pt} = 3787 Hz). HRMS-ESI MS: *m*/*z* 1709.3569 $(M–Cl)^+$. DSC: no maximum observed up to 280 °C. Elemental analysis, calcd for $C_{82}H_{80}P_4Pt_2Cl_4$: C, 57.80; H, 4.62. Found: C, 57.98; H, 4.28.

Data availability

The data supporting this article have been included as part of the ESI.†

Author contributions

S. E. Lindahl and E. M. Metzger carried out the experimental work. Crystallographic data were solved by M. Pink and C.-H. Chen. S. E. Lindahl wrote the manuscript with input from all authors. J. M. Zaleski supervised the work.

Conflicts of interest

There are no conflicts of interest to declare.

Acknowledgements

The generous support of the National Institutes of Health (R01-CA196293) and National Science Foundation (CHE-1265703, CHE-2247314) is gratefully acknowledged. Additionally, this research was supported in part by Lilly Endowment, Inc., through its support for the Indiana University Pervasive Technology Institute. The authors would also like to thank Dr Aurora Clark, Dr Krystyna Kirschner, and Stephen Ratvasky for thoughtful discussions.

References

1 K. Edo, M. Mizugaki, Y. Koide, H. Seto, K. Furihata, N. Otake and N. Ishida, The Structure of Neocarzinostatin Chromophore Possessing a Novel Bicyclo-[7,3,0] Dodecadiyne System, *Tetrahedron Lett.*, 1985, **26**, 331–334.
2 J. Golik, J. Clardy, G. Dubay, G. Groenewold, H. Kawaguchi, M. Konishi, B. Krishnan, H. Ohkuma, K. Saitoh and T. W. Doyle, Esperamicins, A Novel Class of Potent Antitumor Antibiotics. 2. Structure of Esperamicin X, *J. Am. Chem. Soc.*, 1987, **109**, 3461–3462.
3 J. Golik, G. Dubay, G. Groenewold, H. Kawaguchi, M. Konishi, B. Krishnan, H. Ohkuma, K. Saitoh and T. W. Doyle, Esperamicins, A Novel Class of Potent Antitumor Antibiotics. 3. Structures of Esperamicins A1, A2, and A1b, *J. Am. Chem. Soc.*, 1987, **109**, 3462–3464.
4 M. Konishi, H. Ohkuma, K. Matsumoto, T. Tsuno, H. Kamei, T. Miyaki, T. Oki, H. Kawaguchi and A. Dynemicin, A Novel Antibiotic with the Anthraquinone and 1,5-diyn-3-ene Subunit, *J. Antibiot.*, 1989, **42**, 1449–1452.
5 M. D. Lee, T. S. Dunne, C. C. Chang, G. A. Ellestad, M. M. Siegel, G. O. Morton, W. J. McGahren and D. B. Borders, Calichemicins, A Novel Family of Antitumor Antibiotics. 2. Chemistry and Structure of Calichemicin g1, *J. Am. Chem. Soc.*, 1987, **109**, 3466–3468.
6 M. D. Lee, T. S. Dunne, M. M. Siegel, C. C. Chang, G. O. Morton and D. B. Borders, Calichemicins, A Novel Family of Antitumor Antibiotics. 1. Chemistry and Partial Structure of Calichemicin g1, *J. Am. Chem. Soc.*, 1987, **109**, 3464–3466.
7 N. Darby, C. U. Kim, J. A. Salaün, K. W. Shelton, S. Takada and S. Masamune, Concerning the 1,5-Didehydro[10] annulene System, *Chem. Commun.*, 1971, 1516–1517.
8 R. G. Bergman, Reactive 1,4-Dehydroaromatics, *Acc. Chem. Res.*, 1973, **6**, 25–31.
9 S. G. Van Lanen and B. Shen, Biosynthesis of Enediyne Antitumor Antibiotics, *Curr. Top. Med. Chem.*, 2008, **8**, 448–459.
10 B. Shen, Hindra, X. Yan, T. Huang, H. Ge, D. Yang, Q. Teng, J. D. Rudolf and J. R. Lohman, Enediynes: Exploration of

Microbial Genomics to Discover New Anticancer Drug Leads, *Bioorg. Med. Chem. Lett.*, 2015, **25**, 9–15.
11 Z. J. Low, G.-L. Ma, H. T. Tran, Y. Zou, J. Xiong, L. Pang, S. Nuryyeva, H. Ye, J.-F. Hu, K. N. Houk and Z.-X. Liang, Sungeidines from a Non-canonical Enediyne Biosynthetic Pathway, *J. Am. Chem. Soc.*, 2020, **142**, 1673–1679.
12 M. Igarashi, R. Sawa, M. Umekita, M. Hatano, R. Arisaka, C. Hayashi, Y. Ishizaki, M. Suzuki and C. Kato, Sealutomicins, New Enediyne Antibiotics from the Deep-Sea Actinomycete *Nonomuraea* sp. MM565M-173N2, *J. Antibiot.*, 2021, **74**, 291–299.
13 L. Liu, J. Pan, Z. Wang, X. Yan, D. Yang, X. Zhu, B. Shen, Y. Duan and Y. Huang, Ribosome Engineering and Fermentation Optimization Leads to Overproduction of Tiancimycin A, a New Enediyne Natural Product from *Streptomyces* sp. CB03234, *J. Ind. Microbiol. Biotechnol.*, 2018, **45**, 141–151.
14 J. H. Im, D. Shin, Y. H. Ban, W. S. Byun, E. S. Bae, D. Lee, Y. E. Du, J. Cui, Y. Kwon, S.-J. Nam, S. Cha, S. K. Lee, Y. J. Yoon and D.-C. Oh, Targeted Discovery of an Enediyne-Derived Cycloaromatized Compound, Jejucarboside A, from a Marine Actinomycete, *Org. Lett.*, 2022, **24**, 7188–7193.
15 S. Y. Ma, Y. S. Xiao, B. Zhang, F. L. Shao, Z. K. Guo, J. J. Zhang, R. H. Jiao, Y. Sun, Q. Xu, R. X. Tan and H. M. Ge, Amycolamycins A and B, Two Enediyne-Derived Compounds from a Locust-Associated Actinomycete, *Org. Lett.*, 2017, **19**, 6208–6211.
16 D.-C. Oh, P. G. Williams, C. A. Kauffman, P. R. Jensen and W. Fenical, Cyanosporasides A and B, Chloro- and Cyano-cyclopenta[*a*]indene Glycosides from the Marine Actinomycete "*Salinispora pacifica*", *Org. Lett.*, 2006, **8**, 1021–1024.
17 X. Yan, J.-J. Chen, A. Adhikari, D. Yang, I. Crnovcic, N. Wang, C.-Y. Chang, C. Rader and B. Shen, Genome Mining of *Micromonospora yangpuensis* DSM 45577 as a Producer of an Anthraquinone-Fused Enediyne, *Org. Lett.*, 2017, **19**, 6192–6195.
18 Y. Fu and M. Ho, DNA Damaging Agent-Based Antibody-Drug Conjugates for Cancer Therapy, *Antibody Ther.*, 2018, **1**, 43–53.
19 N. K. Damle and P. Frost, Antibody-Targeted Chemotherapy with Immunoconjugates of Calicheamicin, *Curr. Opin. Pharmacol.*, 2003, **3**, 386–390.
20 H. Maeda, SMANCS and Polymer-Conjugated Macromolecular Drugs: Advantages in Cancer Chemotherapy, *Adv. Drug Delivery Rev.*, 2001, **46**, 169–185.
21 H. Maeda, K. Greish and J. Fang, The EPR Effect and Polymeric Drugs: A Paradigm Shift for Cancer Chemotherapy in the 21st Century, *Adv. Polym. Sci.*, 2006, **193**, 103–121.
22 N. Joubert, A. Beck, C. Dumontet and C. Denevault-Sabourin, Antibody-Drug Conjugates: The Last Decade, *Pharmaceuticals*, 2020, **13**, 245–275.
23 K. C. Nicolaou, G. Zuccarello, Y. Ogawa, E. J. Schweiger and T. Kumazawa, Cyclic Conjugated Enediynes Related to Calicheamicins and Esperamicins: Calculations, Synthesis, and Properties, *J. Am. Chem. Soc.*, 1988, **110**, 4866–4868.
24 K. C. Nicolaou, G. Zuccarello, C. Riemer, V. A. Estevez and W.-M. Dai, Design, Synthesis, and Study of Simple Monocyclic Conjugated Enediynes. The 10-Membered Ring Enediyne Moiety of the Enediyne Anticancer Antibiotics, *J. Am. Chem. Soc.*, 1992, **114**, 7360–7371.
25 P. R. Schreiner, Monocyclic Enediynes: Relationships between Ring Sizes, Alkyne Carbon Distances, Cyclization Barriers, and Hydrogen Abstraction Reactions. Singlet-Triplet Separations of Methyl-Substituted p-Benzynes, *J. Am. Chem. Soc.*, 1998, **120**, 4184–4190.
26 J. P. Snyder, The Cyclization of Calicheamicin-Esperamicin Analogues: A Predictive Biradicaloid Transition State, *J. Am. Chem. Soc.*, 1989, **111**, 7630–7632.
27 J. P. Snyder, Monocyclic Enediyne Collapse to 1,4-Diyl Biradicals: A Pathway under Strain Control, *J. Am. Chem. Soc.*, 1990, **112**, 5367–5369.
28 P. Magnus, S. Fortt, T. Pitterna and J. P. Snyder, Synthetic and Mechanistic Studies on Esperamicin A1 and Calichemicin g1. Molecular Strain Rather than p-Bond Proximity Determines the Cycloaromatization Rates of Bicyclo[7.3.1] Enediynes, *J. Am. Chem. Soc.*, 1990, **112**, 4986–4987.
29 M. F. Semmelhack, T. Neu and F. Foubelo, Arene 1,4-Diradical Formation from o-Dialkynylarenes, *Tetrahedron Lett.*, 1992, **33**, 3277–3280.
30 M. F. Semmelhack, T. Neu and F. Foubelo, Arene 1,4-Diradical Formation from o-Dialkynylarenes, *J. Org. Chem.*, 1994, **59**, 5038–5047.
31 G. B. Jones and P. M. Warner, Electronic Control of the Bergman Cyclization: The Remarkable Role of Vinyl Substitution, *J. Am. Chem. Soc.*, 2001, **123**, 2134–2145.
32 G. W. Plourde II, P. M. Warner, D. A. Parrish and G. B. Jones, Halo-Enediynes: Probing the Electronic and Stereoelectronic Contributions to the Bergman Cycloaromatization, *J. Org. Chem.*, 2002, **67**, 5369–5374.
33 M. Schmittel and S. Kiau, Polar Effects in the Transition State of the Bergman Cyclization, *Chem. Lett.*, 1995, 953–954.
34 M. Prall, A. Wittkopp, A. A. Fokin and P. R. Schreiner, Substituent Effects on the Bergman Cyclization of (Z)-1,5-Hexadiyne-3-enes: A Systematic Computational Study, *J. Comput. Chem.*, 2001, **22**, 1605–1614.
35 B. P. Warner, S. P. Millar, R. D. Broene and S. L. Buchwald, Controlled Acceleration and Inhibition of Bergman Cyclization by Metal Chlorides, *Science*, 1995, **269**, 814–816.
36 S. Bhattacharyya, D. F. Dye, M. Pink and J. M. Zaleski, A Geometric Switching Approach toward Thermal Activation of Metalloenediynes, *Chem. Commun.*, 2005, 5295–5297.
37 S. Bhattacharyya, M. Pink, M.-H. Baik and J. M. Zaleski, A Unique Approach to Metal-Induced Bergman Cyclization: Long-Range Enediyne Activation by Ligand-to-Metal Charge Transfer, *Angew. Chem., Int. Ed.*, 2005, **44**, 592–595.
38 T. T. Derencsenyi, Phosphorus-31 Nuclear Magnetic Resonance as a Method of Predicting Ligand Basicity and

Rates of Homogeneous Catalysis, *Inorg. Chem.*, 1981, **20**, 665–670.
39 N. L. Coalter, T. E. Concolino, W. E. Streib, C. G. Hughes, A. L. Rheingold and J. M. Zaleski, Structure and Thermal Reactivity of a Novel Pd(0) Metalloenediyne, *J. Am. Chem. Soc.*, 2000, **122**, 3112–3117.
40 R. H. Grubbs and D. Kratz, Highly Unsaturated Oligomeric Hydrocarbons: a-(Phenylethynyl)-w-phenylpoly[1,2-phenylene(2,1-ethynediyl)], *Chem. Ber.*, 1993, **126**, 149–157.
41 S. E. Lindahl, H. Park, M. Pink and J. M. Zaleski, Utilizing Redox-Mediated Bergman Cyclization toward the Development of Dual-Action Metalloenediyne Therapeutics, *J. Am. Chem. Soc.*, 2013, **135**, 3826–3833.
42 J. D. Spence, A. C. Rios, M. A. Frost, C. M. McCutcheon, C. D. Cox, S. Chavez, R. Fernandez and B. F. Gherman, Syntheses, Thermal Reactivities, and Computational Studies of Aryl-Fused Quinoxalenediynes: Effect of Extended Benzannelation on Bergman Cyclization Energetics, *J. Org. Chem.*, 2012, **77**, 10329–10339.
43 B. P. Warner, *Doctor of Philosophy in Organic Chemistry*, Massachusetts Institute of Technology, 1995.
44 P. J. Benites, D. S. Rawat and J. M. Zaleski, Metalloenediynes: Ligand Field Control of Thermal Bergman Cyclization Reactions, *J. Am. Chem. Soc.*, 2000, **122**, 7208–7217.
45 B. König and W. Pitsch, Synthesis, Structure, and Reactivity of Enediyne Macrocycles, *J. Org. Chem.*, 1996, **61**, 4258–4261.
46 B. König, H. Hollnagel, B. Ahrens and P. G. Jones, Activation of Macrocyclic Biaryl-Enediynes by Metal Ion Coordination, *Angew. Chem., Int. Ed.*, 1995, **34**, 2538–2540.
47 M. R. Porter, S. E. Lindahl, A. Lietzke, E. M. Metzger, Q. Wang, E. Henck, C.-H. Chen, H. Niu and J. M. Zaleski, Metal-Mediated Diradical Tuning for DNA Replication Arrest via Template Strand Scission, *Proc. Natl. Acad. Sci. U. S. A.*, 2017, **114**, E7405–E7414.
48 D. S. Rawat and J. M. Zaleski, Mg^{2+} Induced Thermal Enediyne Cyclization at Ambient Temperature, *J. Am. Chem. Soc.*, 2001, **123**, 9675–9676.
49 D. S. Rawat, P. J. Benites, C. D. Incarvito, A. L. Rheingold and J. M. Zaleski, The Contribution of Ligand Flexibility to Metal Center Geometry Modulated Thermal Cyclization of Conjugated Pyridine and Quinoline Metalloenediynes of Copper(I) and Copper(II), *Inorg. Chem.*, 2001, **40**, 1846–1857.
50 A. Basak and J. C. Shain, Synthesis and Thermal Reactivity of a Novel Macrocyclic Enediyne and its Copper(II) Complex, *Tetrahedron Lett.*, 1998, **39**, 3029–3030.
51 A. Basak, J. C. Shain, U. K. Khamrai, K. R. Rudra and A. Basak, Nitrogen Substituted Cyclic Enediynes: Synthesis, Thermal Reactivity, and Complexation with Metal Ions, *J. Chem. Soc., Perkin Trans. 1*, 2000, 1955–1964.
52 D. L. Boger and J. Zhou, CDPI3-Enediyne and CDPI3-EDTA Conjugates: A New Class of DNA Cleaving Agents, *J. Org. Chem.*, 1993, **58**, 3018–3024.
53 T. Kaneko, M. Takahashi and M. Hirama, Benzannelation Alters the Rate Limiting Step in Enediyne Cycloaromatization, *Tetrahedron Lett.*, 1999, **40**, 2015–2018.
54 S. Koseki, Benzannelation Effect on Enediyne Cycloaromatization: An ab Initio Molecular Orbital Study, *J. Phys. Chem. A*, 1999, **103**, 7672–7675.
55 T. P. Lockhart, P. B. Comita and R. G. Bergman, Kinetic Evidence for the Formation of Discrete 1,4-Dehydrobenzene Intermediates. Trapping by Inter- and Intramolecular Hydrogen Atom Transfer and Observation of High-Temperature CIDNP, *J. Am. Chem. Soc.*, 1981, **103**, 4082–4090.
56 R. K. Mohamed, P. W. Peterson and I. V. Alabugin, Concerted Reactions That Produce Diradicals and Zwitterions: Electronic, Steric, Conformational, and Kinetic Control of Cycloaromatization Processes, *Chem. Rev.*, 2013, **113**, 7089–7129.
57 M. Prall, A. Wittkopp and P. R. Schreiner, Can Fulvenes Form From Enediynes? A Systematic High-Level Computational Study on Parent and Benzannelated Enediyne and Enyne-Allene Cyclizations, *J. Phys. Chem. A*, 2001, **105**, 9265–9274.
58 M. F. Semmelhack and R. Sarpong, Kinetic Analysis of a Reactive Model Enediyne, *J. Phys. Org. Chem.*, 2004, **17**, 807–813.
59 E. C. Sherer, K. N. Kirschner, F. C. Pickard IV, C. Rein, S. Feldgus and G. C. Shields, Efficient and Accurate Characterization of the Bergman Cyclization for Several Enediynes Including an Expanded Substructure of Esperamicin A1, *J. Phys. Chem. B*, 2008, **112**, 16917–16934.
60 T. A. Zeidan, M. Manoharan and I. V. Alabugin, Ortho Effect in the Bergman Cyclization: Interception of p-Benzyne Intermediate by Intramolecular Hydrogen Abstraction, *J. Org. Chem.*, 2006, **71**, 954–961.
61 T. A. Zeidan, S. V. Kovalenko, M. Manoharan and I. V. Alabugin, Ortho Effect in the Bergman Cyclization: Comparison of Experimental Approaches and Dissection of Cycloaromatization Kinetics, *J. Org. Chem.*, 2006, **71**, 962–975.
62 S. A. Valenzuela, A. J. Cortés, Z. J. E. Tippins, M. H. Daly, T. E. Keel, B. F. Gherman and J. D. Spence, Effect of Extended Benzannelation Orientation on Bergman and Related Cyclizations of Isomeric Quinoxalenediynes, *J. Org. Chem.*, 2017, **82**, 13297–13312.
63 T. G. Appleton, H. C. Clark and L. E. Manzer, Trans-Influence. Its Measurement and Significance, *Coord. Chem. Rev.*, 1973, **10**, 335–422.
64 E. Kraka and D. Cremer, CCSD(T) Investigation of the Bergman Cyclization of Enediyne. Relative Stability of o-, m-, and p-Didehydrobezene, *J. Am. Chem. Soc.*, 1994, **116**, 4929–4936.
65 S. Bhattacharyya, A. E. Clark, M. Pink and J. M. Zaleski, Isolation of Electronic from Geometric Contributions to Bergman Cyclization of Metalloenediynes, *Chem. Commun.*, 2003, 1156–1157.
66 A. E. Clark, S. Bhattacharyya and J. M. Zaleski, Density Functional Analysis of Ancillary Ligand Electronic

Contributions to Metal-Mediated Enediyne Cyclization, *Inorg. Chem.*, 2009, **48**, 3926–3933.

67 L. J. K. Boerner, S. Mazumder, M. Pink, M.-H. Baik and J. M. Zaleski, Conformational and Electronic Consequences in Crafting Extended, p-Conjugated, Light-Harvesting Macrocycles, *Chem. –Eur. J.*, 2011, **17**, 14539–14551.

68 E. Kraka and D. Cremer, Enediynes, Enyne-Allenes, Their Reactions, and Beyond, *Wiley Interdiscip. Rev.: Comput. Mol. Sci.*, 2014, **4**, 285–324.

69 I. V. Alabugin and M. Manoharan, Reactant Destabilization in the Bergman Cyclization and Rational Design of Light- and pH-Activated Enediynes, *J. Phys. Chem. A*, 2003, **107**, 3363–3371.

70 M. J. Frisch, G. W. Trucks, H. B. Schlegel, G. E. Scuseria, M. A. Robb, J. R. Cheeseman, G. Scalmani, V. Barone, G. A. Petersson, H. Nakatsuji, X. Li, M. Caricato, A. V. Mrenich, J. Bloino, B. J. Janesko, R. Gomperts, B. Mennucci, H. P. Hratchian, J. V. Ortiz, A. F. Izmaylov, J. L. Sonnenberg, D. Williams-Young, F. Ding, F. Lipparini, F. Egidi, J. Goings, B. Peng, A. Petrone, T. Henderson, D. Rangasinghe, V. G. Zakrewski, J. Gao, N. Rega, G. Zheng, W. Liang, M. Hada, M. Ehara, K. Toyota, R. Fukuda, J. Hasegawa, M. Ishida, T. Nakajima, Y. Honda, O. Kitao, H. Nakai, T. Vreven, K. Throssell, J. A. J. Montgomery, J. E. Peralta, F. Ogliaro, M. Bearpark, J. J. Heyd, E. N. Brothers, K. N. Kudin, V. N. Staroverov, T. A. Keith, R. Kobayashi, J. Normand, K. Raghavachari, A. Rendell, J. C. Burant, S. S. Iyengar, J. Tomasi, M. Cossi, J. M. Millam, M. Klene, C. Adamo, R. Cammi, J. W. Ochterski, R. L. Martin, K. Morokuma, O. Farkas, J. B. Foresman and D. J. Fox, *Gaussian 16*, Revision C.01, Gaussian, Inc. , Wallingford, CT., 2019.

71 A. D. Becke, Density-Functional Exchange-Energy Approximation with Correct Asymptotic Behavior, *Phys. Rev. A*, 1988, **38**, 3098–3100.

72 A. D. Becke, Density-Functional Thermochemistry. III. The Role of Exact Exchange, *J. Chem. Phys.*, 1993, **98**, 5648–5652.

73 C. Lee, W. Yang and R. G. Parr, Development of the Colle-Salvetti Correlation-Energy Formula into a Function of the Electron Density, *Phys. Rev. B*, 1988, **37**, 785–789.

74 S. Grimme, S. Ehrlich and L. Goerigk, Effect of the Damping Function in Dispersion Corrected Density Functional Theory, *J. Comput. Chem.*, 2011, **32**, 1456–1465.

75 K. Burke, J. P. Perdew and Y. Wang, *Electronic Density Functional Theory: Recent Progress and New Directions*, Plenum, 1998.

76 J. P. Perdew, *Electronic Structure of Solids '91*, Akademie Verlag, Berlin, 1991.

77 J. P. Perdew, K. Burke and Y. Wang, Generalized Gradient Approximation for the Exchange-Correlation Hole of a Many-Electron System, *Phys. Rev. B: Condens. Matter Mater. Phys.*, 1996, **54**, 16533–16539.

78 J. P. Perdew, J. A. Chevary, S. H. Vosko, K. A. Jackson, M. R. Pederson, D. J. Singh and C. Fiolhais, Atoms, Molecules, Solids, and Surfaces: Applications of the Generalized Gradient Approximation for Exchange and Correlation, *Phys. Rev. B: Condens. Matter Mater. Phys.*, 1992, **46**, 6671–6687.

79 J. P. Perdew, J. A. Chevary, S. H. Vosko, K. A. Jackson, M. R. Pederson, D. J. Singh and C. Fiolhais, Erratum: Atoms, Molecules, Solids, and Surfaces: Applications of the Generalized Gradient Approximation for Exchange and Correlation, *Phys. Rev. B: Condens. Matter Mater. Phys.*, 1993, **48**, 4978.

80 P. J. Hay and W. R. Wadt, Ab Initio Effective Core Potentials for Molecular Calculations. Potentials for the Transition Metal Atoms Sc to Hg, *J. Chem. Phys.*, 1985, **82**, 270–283.

81 P. J. Hay and W. R. Wadt, Ab Initio Effective Core Potentials for Molecular Calculations. Potentials for K to Au Including the Outermost Core Orbitals, *J. Chem. Phys.*, 1985, **82**, 299–310.

82 W. R. Wadt and P. J. Hay, Ab Initio Effective Core Potentials for Molecular Calculations. Potentials for Main Group Elements Na to Bi, *J. Chem. Phys.*, 1985, **82**, 284–298.

83 C. J. Cramer, Bergman, Aza-Bergman, and Protonated Aza-Bergman Cyclizations and Intermediate 2,5-Arynes: Chemistry and Challenges to Computation, *J. Am. Chem. Soc.*, 1998, **120**, 6261–6269.

84 M. Cossi, V. Barone, R. Cammi and J. Tomasi, Ab Initio Study of Solvated Molecules: A New Implementation of th Polarizable Continuum Model, *Chem. Phys. Lett.*, 1996, **255**, 327–335.

85 S. Miertus, E. Scrocco and J. Tomasi, Electrostatic Interaction of a Solute with a Continuum. A Direct Utilization of Ab Initio Molecular Potentials for the Prevision of Solvent Effects, *Chem. Phys.*, 1981, **55**, 117–129.

86 S. Miertus and J. Tomasi, Approximate Evaluations of the Electrostatic Free Energy and Internal Energy Changes in Solution Processes, *Chem. Phys.*, 1982, **65**, 239–245.

87 J. L. Pascual-Ahuir, E. Silla and I. Tuñón, GEPOL: An Improved Description of Molecular Surfaces. III. A New Algorithm for the Computation of a Solvent-Excluding Surface, *J. Comput. Chem.*, 1994, **15**, 1127–1138.

88 J. Tomasi, B. Mennucci and R. Cammi, Quantum Mechanical Continuum Solvation Models, *Chem. Rev.*, 2005, **105**, 2999–3093.

89 M.-T. Béraldin, E. Vauthier and S. Fliszár, Charge Distributions and Chemical Effects. XXVI. Relationships Between Nuclear Magnetic Resonance Shifts and Atomic Charges for 17O Nuclei in Ethers and Carbonyl Compounds, *Can. J. Chem.*, 1982, **60**, 106–110.

90 S. Fliszár, G. Cardinal and M.-T. Béraldin, Charge Distributions and Chemical Effects. 30. Relationship Between Nuclear Magnetic Resonance Shifts and Atomic Charges, *J. Am. Chem. Soc.*, 1982, **104**, 5287–5292.

91 H. Henry and S. Fliszár, Charge Distributions and Chemical Effects. 13. Ab Initio Study of the Charge Density-13C Nuclear Magnetic Resonance Shift Correlation for Ethylenic Carbon Atoms, *J. Am. Chem. Soc.*, 1978, **100**, 3312–3315.

92 I. V. Alabugin, in *Stereoelectronic Effects: A Bridge Between Structure and Reactivity*, 2016, pp. 322–375, DOI: **10.1002/9781118906378.ch12**.

93 U. Rosenthal, G. Oehme, V. V. Burlakov, P. V. Petrovskii, V. B. Shur and M. E. Vol'pin, Carbon-13 and Proton NMR Studies of Selected Transition Metal Alkyne Complexes, *J. Organomet. Chem.*, 1990, **391**, 119–122.
94 M. Karplus and J. A. Pople, Theory of Carbon NMR Chemical Shifts in Conjugated Molecules, *J. Chem. Phys.*, 1963, **38**, 2803–2807.
95 K. M. Kirschner, S. C. Ratvasky, M. Pink and J. M. Zaleski, Anion Control of Lanthanoenediyne Cyclization, *Inorg. Chem.*, 2019, **58**, 9225–9235.
96 M. Rubin, A. Trofimov and V. Gevorgyan, Can Polarization of Triple Bond in Tolanes Be Deduced from 13C NMR Shifts? Re-evaluation of Factors Affecting Regiochemistry of the Palladium-Catalyzed Hydrostannation of Alkynes, *J. Am. Chem. Soc.*, 2005, **127**, 10243–10249.
97 E. Kleinpeter and A. Schulenburg, Quantification of the Push-Pull Effect in Tolanes and a Revaluation of the Factors Affecting the ^{13}C Chemical Shifts of the Carbon Atoms of the C-C Triple Bond, *J. Org. Chem.*, 2006, **71**, 3869–3875.
98 N. Nardangeli, N. Topolovčan, R. Simionescu and T. Hudlicky, Polarization Effect on Regioselectivity of Pd-Catalyzed Cyclization of 2-Alkynylbenzaldehydes, *Eur. J. Org Chem.*, 2020, 227–233.
99 J. Gräfenstein, E. Kraka, M. Filatov and D. Cremer, Can Unrestricted Density-Functional Theory Describe Open Shell Singlet Biradicals?, *Int. J. Mol. Sci.*, 2002, **3**, 360–394.
100 W. E. Slinkard and D. W. Meek, Co-ordination Properties of Methylenebis(diphenylphosphine chalcogenides) with Cobalt(II), Nickel(II), and Palladium(II), *J. Chem. Soc., Dalton Trans.*, 1973, 1024–1027.